

FERMILAB-Pub-00/153-T
UB-HET-00-01
August 2000

Probing Neutral Gauge Boson Self-interactions in ZZ Production at Hadron Colliders

U. Baur*

Department of Physics, State University of New York, Buffalo, NY 14260, USA

D. Rainwater†

Theory Group, Fermi National Accelerator Laboratory, Batavia, IL 60510, USA

Abstract

A detailed analysis of ZZ production at the upgraded Fermilab Tevatron and the CERN Large Hadron Collider is presented for general ZZZ and $ZZ\gamma$ couplings. Deviations from the Standard Model gauge theory structure for each of these can be parameterized in terms of two form factors which are severely restricted by unitarity at high energy. Achievable limits on these couplings are shown to be a dramatic improvement over the limits currently obtained by e^+e^- experiments.

*e-mail: baur@ubhex.physics.buffalo.edu

†e-mail: dlrain@fnal.gov

I. INTRODUCTION

The Standard Model (SM) of electroweak interactions makes precise predictions for the couplings between gauge bosons due to the non-abelian gauge symmetry of $SU(2)_L \otimes U(1)_Y$. These self-interactions are described by the triple gauge boson (trilinear) WWV , $Z\gamma V$, and ZZV ($V = \gamma, Z$) couplings and the quartic couplings. Vector boson pair production provides a sensitive ground for *direct tests* of the trilinear couplings. Deviations of the couplings from the expected values would indicate the presence of new physics beyond the SM.

To date the SM has passed this rigorous test with no observed deviations from the SM values. The WWV couplings have been measured with an accuracy of 10 – 15% in W^+W^- , single photon and single W production at LEP2 [1], and with 20 – 40% accuracy in $W\gamma$, WZ and W^+W^- production at the Fermilab Tevatron collider [2–5]. The $Z\gamma V$ couplings can be probed in $Z\gamma$ production in e^+e^- and in hadronic collisions. The LEP2 [1] and Tevatron [6,7] experiments find the $Z\gamma V$ couplings to be smaller than 0.05 – 0.4, depending on the specific coupling considered. The ZZV couplings, on the other hand, are only loosely constrained at the moment through ZZ production at LEP2 [1]. Due to low event rates after branching ratios, or large backgrounds, ZZ production was not observed by the Tevatron experiments in Run I.

In Run II of the Tevatron which will begin in 2001, an integrated luminosity of 2 – 15 fb⁻¹ is envisioned [8], and a sufficient number of ZZ events should be available to commence a detailed investigation of the ZZV couplings. At the CERN Large Hadron Collider [(LHC), pp collisions at $\sqrt{s} = 14$ TeV [9]], one can imagine that the measurement of these couplings reaches the 0.1% level of current precision electroweak data. In this paper we study the capabilities of future hadron collider experiments to test the ZZV vertices via ZZ production. In the past, the reaction $p\bar{p} \rightarrow ZZ$ for non-zero ZZV couplings has only been studied in the approximation where the Z bosons are considered as stable final state particles [10,11]. We go a step further and include Z decays with full decay correlations, finite Z width effects and time-like virtual photon exchange in our analysis.

Two ZZZ couplings, and two $ZZ\gamma$ couplings, are allowed by electromagnetic gauge invariance and Lorentz invariance [12] for on-shell Z bosons. We discuss the properties of these couplings in Section II, where we also derive unitarity bounds for the form factors associated with the ZZV vertices. The SM is assumed to be valid in our calculations except for the ZZV anomalous couplings; Vff couplings and strong interactions of SM particles remain unchanged.

Our analysis examines the observable final state signatures at hadron colliders, $ZZ \rightarrow \ell_1^+ \ell_1^- \ell_2^+ \ell_2^-$, $\ell^+ \ell^- \nu \bar{\nu}$, $\ell^+ \ell^- jj$ ($\ell, \ell_1, \ell_2 = e, \mu$) and $\bar{\nu} \nu jj$. In Section III we provide details of the signal and various backgrounds and discuss the signatures of anomalous ZZZ and $ZZ\gamma$ couplings. Besides the ZZ invariant mass distribution and the Z boson transverse momentum distributions, the azimuthal angle between the Z boson decay fermions, $\Delta\Phi$, and their separation in the pseudo-rapidity – azimuthal angle plane, ΔR , are sensitive indicators of anomalous couplings. The $\Delta\Phi$ distribution may be useful in discriminating different types of ZZV couplings, and in determining their sign. In Section IV we derive sensitivity limits for anomalous ZZV couplings for various integrated luminosities at the Tevatron and LHC and discuss the results. Finally, in Section V we compare the expectations for Tevatron Run II and the LHC with the current LEP2 limits and expectations for an e^+e^- Linear

Collider. In Section V we also present our conclusions.

II. ZZZ AND ZZ γ ANOMALOUS COUPLINGS

In the SM, at the parton level, the reaction $p\bar{p} \rightarrow ZZ$ proceeds by the Feynman diagrams of Fig. 1. Including the anomalous couplings under discussion requires the addition of the graphs of Fig. 2. In the massless fermion limit, a reasonable approximation for hadron collider processes, the most general form of the $Z^\alpha(q_1) Z^\beta(q_2) V^\mu(P)$ ($V = Z, \gamma$) vertex function (see Fig. 3 for notation) for on-shell Z 's which respects Lorentz invariance and electromagnetic gauge invariance may be written as [12]

$$g_{ZZV} \Gamma_{ZZV}^{\alpha\beta\mu} = e \frac{P^2 - M_V^2}{M_Z^2} \left[i f_4^V (P^\alpha g^{\mu\beta} + P^\beta g^{\mu\alpha}) + i f_5^V \epsilon^{\mu\alpha\beta\rho} (q_1 - q_2)_\rho \right], \quad (1)$$

where M_Z is the Z -boson mass and e is the proton charge. The overall factor $(P^2 - M_V^2)$ in Eq. (1) is a consequence of Bose symmetry for ZZZ couplings, while it is due to electromagnetic gauge invariance for the $ZZ\gamma$ couplings. The couplings f_i^V ($i = 4, 5$) are dimensionless complex functions of q_1^2 , q_2^2 and P^2 . All couplings are C odd; CP invariance forbids f_4^V and parity conservation requires that f_5^V vanishes. Because f_4^Z and f_4^γ are CP -odd, contributions to the helicity amplitudes proportional to these couplings will not interfere with the SM terms. In the static limit, f_5^γ corresponds to the anapole moment of the Z boson [13]. In the SM, at tree level, $f_4^V = f_5^V = 0$. At the one-loop level, only the CP conserving couplings f_5^V receive contributions. Numerically, these contributions are of $\mathcal{O}(10^{-4})$ [14]. Loop contributions from supersymmetric particles and additional heavy fermions produce ZZV couplings of a similar magnitude [14]. If the Z bosons are allowed to be off-shell, five additional ZZZ couplings, and five additional $ZZ\gamma$ couplings contribute [15]. For these couplings, the factor $(P^2 - M_V^2)$ in the vertex function is replaced by $(q_1^2 - q_2^2)$. The effect of these couplings thus is strongly suppressed and we shall ignore them in our discussion.

It should be noted that the two $ZZ\gamma$ couplings contributing to ZZ production are completely independent of the four $Z\gamma Z$ couplings which appear in $Z\gamma$ production (assuming that the Z -boson is on-shell). If all three vector bosons in the vertex function are off-shell, there are seven couplings altogether. Four of them survive in $Z\gamma$ production, and two in $f\bar{f} \rightarrow ZZ$.

The parton level di-boson production cross sections with non-SM couplings manifestly grow with the parton center of mass energy $\sqrt{\hat{s}}$. S -matrix unitarity restricts the ZZV couplings uniquely to their SM values at asymptotically high energies [16]. This requires that the couplings f_i^V possess a momentum dependence which ensures that the $f_i^V(q_1^2, q_2^2, P^2)$ vanish for any momenta much larger than M_Z . For ZZ production, $q_1^2, q_2^2 \sim M_Z^2$ even considering finite Z width effects, but $P^2 = \hat{s}$ may be quite large at the hadron colliders under consideration. In order to avoid unphysical results that would violate unitarity, the \hat{s} dependence thus has to be taken into account. To parameterize the \hat{s} dependence of the form factor, we will use a generalized dipole form factor [17],

$$f_i^V(\hat{s}) = \frac{f_{i0}^V}{(1 + \hat{s}/\Lambda_{FF}^2)^n} \quad (i = 4, 5), \quad (2)$$

where Λ_{FF} is the form factor scale which is related to the scale of the new physics which is generating the anomalous ZZV couplings.

The values $f_{i0}^V = f_i^V(M_Z^2, M_Z^2, 0)$ of the form factors at low energy ($\hat{s} = 0$) and the power of the form factor, n , are constrained by partial wave unitarity of the inelastic ZZ production amplitude in fermion antifermion annihilation at arbitrary center-of-mass energies. In deriving unitarity limits for the f_{i0}^V 's, we follow the strategy employed in Ref. [18]. The anomalous contribution to the

$$f(\sigma)\bar{f}(\bar{\sigma}) \rightarrow Z(\lambda_1)Z(\lambda_2) \quad (3)$$

helicity amplitudes may be written as

$$\Delta\mathcal{M}^V(\sigma\bar{\sigma}, \lambda_1\lambda_2) = -\sqrt{2} e^2 g_{2\sigma}^{Vf_1f_2} \frac{\hat{s}}{M_Z^2} \beta \delta_{\sigma,\bar{\sigma}} A_{\lambda_1\lambda_2}^V \times d_{\sigma+\bar{\sigma}, \lambda_1-\lambda_2}^1(\Theta), \quad (4)$$

where d^1 are the conventional d -functions [19], $\beta = (1 - 4M_Z^2/\hat{s})^{1/2}$, $\sigma, \bar{\sigma}$ and λ_1, λ_2 are the helicities of the incoming fermion pair and outgoing Z pair, respectively. $g_{2\sigma}^{Vf_1f_2}$ is the coupling of the s -channel vector boson to the incoming fermion pair, Θ is the center of mass scattering angle, and the A^V 's are the reduced amplitudes given by (see also Ref. [20])

$$A_{0\pm}^V = \frac{\sqrt{\hat{s}}}{2M_Z} [-if_4^V \pm \beta f_5^V], \quad (5)$$

$$A_{\pm 0}^V = \frac{\sqrt{\hat{s}}}{2M_Z} [if_4^V \mp \beta f_5^V], \quad (6)$$

$$A_{\pm\pm}^V = A_{00}^V = A_{\pm\mp}^V = 0. \quad (7)$$

Examination of the $J = 1$ partial wave amplitude produces the desired unitarity bounds,

$$\left(\sum_{\lambda_1\lambda_2} |A_{\lambda_1\lambda_2}^\gamma|^2 \right)^{1/2} \leq \frac{1}{\alpha\beta^{3/2}} \left[\frac{3}{5} (3 - 6\sin^2\theta_W + 8\sin^4\theta_W) \right]^{1/2} \frac{M_Z^2}{\hat{s}}, \quad (8)$$

$$\left(\sum_{\lambda_1\lambda_2} |A_{\lambda_1\lambda_2}^Z|^2 \right)^{1/2} \leq \frac{4}{\alpha\beta^{3/2}} \sqrt{\frac{3}{10}} \sin\theta_W \cos\theta_W \frac{M_Z^2}{\hat{s}}, \quad (9)$$

where θ_W is the weak mixing angle and α the QED fine structure constant.

By substituting Eq. (2) and assuming that only one coupling is nonzero at a time, we find the following unitarity bounds for $\Lambda_{FF} \gg M_Z$:

$$|f_{40,50}^\gamma| \leq \frac{1}{\alpha} \left[\frac{3}{5} (3 - 6\sin^2\theta_W + 8\sin^4\theta_W) \right]^{1/2} \left(\frac{M_Z}{\Lambda_{FF}} \right)^3 \frac{\left(\frac{2}{3}n \right)^n}{\left(\frac{2}{3}n - 1 \right)^{(n-3/2)}}, \quad (10)$$

$$|f_{40,50}^Z| \leq \frac{4}{\alpha} \sqrt{\frac{3}{10}} \sin\theta_W \cos\theta_W \left(\frac{M_Z}{\Lambda_{FF}} \right)^3 \frac{\left(\frac{2}{3}n \right)^n}{\left(\frac{2}{3}n - 1 \right)^{(n-3/2)}}. \quad (11)$$

Tree level unitarity is satisfied throughout the entire \hat{s} range when these limits are observed. For the more likely case that several anomalous couplings contribute, cancellations may

occur and the bounds are weaker than those listed in Eqs. (10) and (11). From the n dependent factors in (10) and (11) one observes that $n > 3/2$ is necessary in order to satisfy unitarity. This is a direct consequence of the high energy behavior of the anomalous contributions to the ZZ helicity amplitudes, which grow like $(\sqrt{s}/M_Z)^3$. In the following we shall assume that $n = 3$. Selecting an exponent sufficiently above the minimum value of $3/2$ ensures that the ZZ differential cross section stays well below the unitarity limit at energies $\sqrt{s} \gg \Lambda_{FF} \gg M_Z$, where novel phenomena such as resonance production, or multiple weak boson production, are expected to dominate. For the form factor scale we choose $\Lambda_{FF} = 750$ GeV at the Tevatron and $\Lambda_{FF} = 2$ TeV at the LHC in our numerical simulations.

III. SIGNATURES OF ANOMALOUS ZZV COUPLINGS

In this section we discuss characteristics of the signal and backgrounds of anomalous ZZV couplings. For simplicity, we consider only real ZZV couplings. We consider four signatures of ZZ production: decays to four leptons; two leptons and missing energy; two leptons and two jets; and two jets plus missing energy. Due to the overwhelming four jet QCD background, decays where both Z bosons decay hadronically are not considered here. We calculate the SM signal, the signal with anomalous couplings, and the significant backgrounds via full tree level matrix elements for the subprocess in question, each of which is discussed in detail below.

A. General considerations

Our calculation is carried out at the tree level. We compute the $q\bar{q} \rightarrow ZZ \rightarrow 4$ fermion helicity amplitudes in the double pole approximation which ignores contributions from non-resonant diagrams except for contributions from time-like photon exchange diagrams, using the method described in Ref. [21]. Decay correlations, finite Z width effects and contributions from time-like photon exchange are taken into account. Cross sections and dynamical distributions are evaluated using a parton level Monte Carlo program.

To simulate the effect of next-to-leading-log (NLL) QCD corrections we multiply the differential cross section with a simple K -factor which depends on the final state considered. A more detailed discussion of how NLL QCD corrections affect the four different final states is presented in the following sections, where we discuss each final state in turn. Gluon fusion, $gg \rightarrow ZZ$, contributes about 1% (15%) to the cross section at the Tevatron (LHC) [22]. We do not include the contribution from gluon fusion into our analysis.

To examine the effects of anomalous couplings on observables we simulate $p\bar{p}$ (pp) collisions at $\sqrt{s} = 2$ TeV ($\sqrt{s} = 14$ TeV) for the Tevatron (LHC). For all our numerical results we have chosen the set of SM input parameters to be: $\sin^2 \theta_W = 0.2310$, $M_Z = 91.187$ GeV, and $\alpha(M_Z) = 1/128.93$ [23]. For all processes which depend on the QCD coupling constant, we choose the value of the strong coupling constant to be $\alpha_s(M_Z) = 0.118$. We employ CTEQ4L parton distribution functions [24] for all calculations, selecting the value of the factorization scale to be $\mu_f = M_Z$.

As finite detector resolution can have a sizable effect on cross sections and thus the number of events accepted into the data set, to make our calculations realistic we must take into account some minimal detector response. We accomplish this via Gaussian smearing of the four momenta of the outgoing particles according to detector expectations. For Gaussian smearing at the Tevatron we use the expected values of the upgraded CDF detector [25]:

$$\begin{aligned}\frac{\Delta E}{E}(\text{had}) &= \frac{0.75}{\sqrt{E_T}} \oplus 0.03 \quad (|\eta| < 1.1) \\ &= \frac{0.80}{\sqrt{E}} \oplus 0.05 \quad (|\eta| > 1.1) \\ \frac{\Delta E}{E}(\text{lep}) &= \frac{0.14}{\sqrt{E_T}} \oplus 0.02 \quad (|\eta| < 1.1) \\ &= \frac{0.16}{\sqrt{E}} \oplus 0.01 \quad (|\eta| > 1.1)\end{aligned}$$

For the LHC we take the expected values for the ATLAS detector [26]:

$$\begin{aligned}\frac{\Delta E}{E}(\text{had}) &= \frac{0.5}{\sqrt{E}} \oplus 0.03 \quad (|\eta| < 3.0) \\ \frac{\Delta E}{E}(\text{lep}) &= \frac{0.095}{\sqrt{E}} \oplus 0.005 \quad (|\eta| < 2.5)\end{aligned}$$

Here, η is the pseudo-rapidity, E (E_T) is the energy (transverse energy) measured in GeV, and the \oplus sign symbolizes that the two terms are added in quadrature.

In all cases, the missing momentum in an event is taken as the negative vector sum of the smeared four momenta of all observable final state particles. This does ignore the effects of additional soft activity that will affect this distribution in experiment, but for our purposes here may be safely neglected.

The geometric and kinematic acceptance of detectors, i.e. the ability to observe and properly identify final states particles, is simulated in our calculations by cuts imposed on observable particles in the final state. At the Tevatron (LHC) we require ($\ell = e, \mu$):

Tevatron	LHC
$p_T(\ell) > 15 \text{ GeV}$	$p_T(\ell) > 15 \text{ GeV}$
$ \eta(\ell) < 2.5$	$ \eta(\ell) < 2.5$
$p_T(j) > 20 \text{ GeV}$	$p_T(j) > 30 \text{ GeV}$
$ \eta(j) < 2.5$	$ \eta(j) < 3$
$\Delta R(\ell j) > 0.6$	$\Delta R(\ell j) > 0.6$
$\Delta R(jj) > 0.6$	$\Delta R(jj) > 0.6$
$\not{p}_T > 20 \text{ GeV}$ for $ZZ \rightarrow \ell^+ \ell^- \bar{\nu} \nu$	$\not{p}_T > 50 \text{ GeV}$ for $ZZ \rightarrow \ell^+ \ell^- \bar{\nu} \nu$
$\not{p}_T > 60 \text{ GeV}$ for $ZZ \rightarrow \bar{\nu} \nu jj$	$\not{p}_T > 60 \text{ GeV}$ for $ZZ \rightarrow \bar{\nu} \nu jj$

where p_T is the transverse momentum and

$$\Delta R = [(\Delta\Phi)^2 + (\Delta\eta)^2]^{1/2} \quad (12)$$

is the separation in the pseudorapidity – azimuthal angle plane. \not{p}_T is the missing transverse momentum resulting from the nonobservation of the neutrino pair.

In addition, we require the $\ell^+\ell^-$ and two jet invariant masses to be within ± 15 GeV of the Z boson mass [27,28]:

$$76 \text{ GeV} < m(\ell^+\ell^-) < 106 \text{ GeV}, \quad (13)$$

$$76 \text{ GeV} < m(jj) < 106 \text{ GeV}. \quad (14)$$

These cuts help suppress contributions from non-resonant Feynman diagrams and, in the jet case, the background from $Z + 2$ jet production. Additional cuts which are imposed to reduce backgrounds for individual final states will be discussed when we consider the specific final state to which they apply.

B. The $\ell_1^+\ell_1^-\ell_2^+\ell_2^-$ channel

The first ZZ decay channel we consider, $ZZ \rightarrow \ell_1^+\ell_1^-\ell_2^+\ell_2^-$ ($\ell_1, \ell_2 = e, \mu$) is observationally the cleanest as it is essentially background-free. However, it does suffer from a small event rate due to a tiny branching ratio of $B(ZZ \rightarrow \ell_1^+\ell_1^-\ell_2^+\ell_2^-) = 0.0045$ if both electron and muon final states are considered. In the following we concentrate on the $ZZ \rightarrow e^+e^-\mu^+\mu^-$ channel. Results for the $e^+e^-e^+e^-$ and $\mu^+\mu^-\mu^+\mu^-$ final states can be obtained by dividing all cross section results by two. However, for these final states one has to take into account the combinatorial background originating from not being able experimentally to distinguish identical charged leptons. All results presented in this section include a K -factor of 1.28 (1.34) at Tevatron (LHC) energies to approximate the effect of NLL QCD corrections [29]. Inclusive NLL QCD corrections to ZZ production are known to modify the shape of distributions only insignificantly. As mentioned in Sec. III A, we do not include the non-resonant Feynman diagrams which contribute to $q\bar{q} \rightarrow e^+e^-\mu^+\mu^-$ in our calculation. Requiring the invariant mass of the lepton pairs to be in the vicinity of the Z mass, (see Eq. (13)), these diagrams contribute less than a few percent to the differential cross section. Imposing the cuts listed in Sec. III A, one obtains a $ZZ \rightarrow \ell^+\ell^-\ell^+\ell^-$ ($\ell = e, \mu$) cross section of 3.85 fb (22.5 fb) at the Tevatron (LHC). For 2 fb $^{-1}$ in Run II, only a few $ZZ \rightarrow 4$ lepton events are therefore expected within the framework of the SM.

Similar to the WWV and $Z\gamma V$ couplings [12,17], the effects of anomalous ZZV couplings are enhanced at large energies. A typical signal of nonstandard ZZZ and $ZZ\gamma$ couplings thus will be a broad increase in the ZZ invariant mass distribution, the Z transverse momentum distribution and the p_T distribution of the Z decay products. The $p_T(Z)$ and $p_T(\mu)$ distributions for the Tevatron ($p\bar{p}$ collisions at $\sqrt{s} = 2$ TeV) and the LHC are shown in Figs. 4 and 5, respectively. Results are shown for the SM and two ZZV couplings, $f_{40}^Z = 0.3$ (0.02) and $f_{50}^\gamma = -0.3$ (-0.02) at the Tevatron (LHC). Here, and in all subsequent figures, only one ZZV coupling is allowed to be non-zero at a time.

Terms proportional to f_4^V and f_5^V in the matrix elements have identical high energy behavior. Differences in the differential cross sections at high energies between ZZZ and $ZZ\gamma$ couplings are thus controlled by the $Zf\bar{f}$ and $\gamma f\bar{f}$ couplings, and by the parton distribution functions. At the Tevatron these result in differential cross sections which differ by only a few percent for $\hat{s} \gg M_Z^2$ if $|f_{i0}^Z| = |f_{i0}^\gamma|$ ($i = 4, 5$). Slightly larger differences are observed at

intermediate energies and transverse momenta. Since f_4^V violate CP conservation, terms in the helicity amplitudes proportional to those couplings do not interfere with the SM terms. Cross sections thus are independent of the sign of f_4^V . Interference effects between the anomalous and SM contributions to the helicity amplitudes, however, do occur for f_5^V . The magnitude of the interference effects in the transverse momentum and ZZ invariant mass distributions unfortunately is small.

While it would be difficult to discriminate between the various ZZV couplings in the m_{ZZ} or p_T distributions, it should be easy to distinguish between the SM Higgs boson which decays in a pair of Z bosons, $H \rightarrow ZZ$, and anomalous ZZV couplings. This will be important at the LHC, where final states resulting from $pp \rightarrow ZZ$ are prime Higgs boson search channels. Anomalous gauge boson couplings lead to a broad increase in the differential cross section at large energies and transverse momenta, whereas a scalar resonance produces a Breit-Wigner resonance in the m_{ZZ} distribution and a Jacobian peak in the $p_T(Z)$ spectrum. In addition, the correlation of the angular distributions of the Z decay leptons in the Z boson rest frames may be used to discriminate between a Higgs boson and ZZV couplings. Z bosons originating from Higgs boson decay are mostly longitudinally polarized [30], whereas anomalous ZZV couplings lead to one transversely polarized and one longitudinally polarized Z boson (see Eqs. (5) and (6)). Since the Z boson coupling to charged leptons is almost purely axial vector like, transversely polarized Z bosons lead to an angular distribution for the Z decay leptons which is proportional to $(1 + \cos^2 \theta^*)$, where θ^* is the polar angle in the Z boson rest frame with respect to the flight direction of the Z boson in the ZZ rest frame. On the other hand, the angular distribution for longitudinal Z 's is proportional to $\sin^2 \theta^*$.

In order to distinguish f_4^V and f_5^V , and to determine the sign of f_5^V , the ΔR distribution and the distribution of the opening angle in the transverse plane, $\Delta\Phi$, of the $\ell^+\ell^-$ pair originating from the decay of a Z boson may be helpful, if deviations from the SM predictions are found in the m_{ZZ} and the transverse momentum differential cross sections. Figure 6 shows the $\Delta R(\mu^+\mu^-)$ and $\Delta\Phi(\mu^+\mu^-)$ distributions for $ZZ \rightarrow e^+e^-\mu^+\mu^-$ at the Tevatron in the SM and for non-standard ZZZ couplings. Similar results are obtained for the corresponding distributions of the e^+e^- pair, and for the $ZZ\gamma$ couplings $f_{4,5}^\gamma$. The SM $\Delta R(\mu^+\mu^-)$ and $\Delta\Phi(\mu^+\mu^-)$ differential cross sections are dominated by the threshold region, $\sqrt{s} \approx 2M_Z$, where the Z boson momenta are small and the decay leptons tend to be back-to-back, i.e. the distributions are strongly peaked at $\Delta R \approx 3$ and $\Delta\Phi = 180^\circ$. Anomalous couplings affect the cross section mostly at large Z -boson transverse momentum. Due to the Lorentz boost, the relative opening angle between the leptons originating from $Z \rightarrow \ell^+\ell^-$ decreases with increasing p_T . The deviations due to non-standard ZZV couplings in the $\Delta R(\mu^+\mu^-)$ and $\Delta\Phi(\mu^+\mu^-)$ distributions are therefore concentrated at rather small values. Figure 6 demonstrates that the $\Delta\Phi(\mu^+\mu^-)$ distribution would be particularly useful in separating the individual ZZV couplings. The shapes of the $\Delta\Phi(\mu^+\mu^-)$ distributions for $f_{40}^Z = 0.3$, $f_{50}^Z = 0.3$ and $f_{50}^Z = -0.3$ differ considerably, and for a sufficient number of events it should be possible to distinguish f_4^V from f_5^V , and to determine the sign of f_5^V . Unfortunately, both the $\Delta R(\mu^+\mu^-)$ and the $\Delta\Phi(\mu^+\mu^-)$ differential cross sections are useless in distinguishing f_i^Z from f_i^γ ($i = 4, 5$). As for the ZZ invariant mass distribution and the transverse momentum distributions, the differential cross sections for $f_i^Z = f_i^\gamma$ differ very little in shape and magnitude.

At the Tevatron, the small number of $ZZ \rightarrow 4$ leptons events will limit the usefulness

of the $\Delta R(\ell^+\ell^-)$ and $\Delta\Phi(\ell^+\ell^-)$ distributions. At the LHC, the expected number of events is much larger; however, the magnitude of the interference effects between the SM and the anomalous contributions to the helicity amplitudes is significantly smaller than at the Tevatron. This can be easily understood from the high energy behavior of the anomalous contributions to the differential cross section. The differential cross section is proportional to the squared amplitude, which contains the SM terms, terms linear in the anomalous couplings and terms which are quadratic in the ZZV couplings. The terms linear in the anomalous couplings originate from the interference between the SM amplitude and the anomalous contributions, and are proportional to $(\sqrt{\hat{s}}/M_Z)^3$. Terms quadratic in the ZZV couplings on the other hand are proportional to $(\hat{s}/M_Z^2)^3$ and thus grow much faster with \hat{s} . Due to the much higher parton center of mass energies accessible at the LHC, interference effects thus play a smaller role than at the Tevatron. The $\Delta R(\mu^+\mu^-)$ and the $\Delta\Phi(\mu^+\mu^-)$ distributions at the LHC for the SM, $f_{40}^Z = 0.02$, $f_{50}^Z = 0.02$, and $f_{50}^Z = -0.02$ are shown in Fig. 7. Both distributions are very insensitive to the sign of f_{50}^Z . The shape of the $\Delta\Phi(\mu^+\mu^-)$ distribution differs for f_{40}^Z and f_{50}^Z for $\Delta\Phi(\mu^+\mu^-) < 20^\circ$, whereas the $\Delta R(\mu^+\mu^-)$ distributions for f_{40}^Z and f_{50}^Z values of equal magnitude are almost identical. It would thus be challenging to discriminate between f_4^V and f_5^V , and to determine the sign of f_5^V , using the $\Delta R(\ell^+\ell^-)$ and the $\Delta\Phi(\ell^+\ell^-)$ distributions in the $ZZ \rightarrow 4$ leptons mode at the LHC. Since events in regions where anomalous ZZV couplings have a significant effect originate from higher values of $\sqrt{\hat{s}}$, the typical separation and the opening angle in the transverse plane are significantly smaller than at the Tevatron.

C. The $\ell^+\ell^-\bar{\nu}\nu$ channel

In contrast to the $ZZ \rightarrow 4$ leptons mode which is almost background free, there are several potentially important background processes if one of the two Z bosons decays into neutrinos. The advantage of the $ZZ \rightarrow \ell^+\ell^-\bar{\nu}\nu$ channel, observable as $\ell^+\ell^-\cancel{p}_T$, is its larger branching fraction. Summing over the three neutrino species, the raw number of $ZZ \rightarrow \ell^+\ell^-\bar{\nu}\nu$ signal events before cuts are implemented is about a factor 6 larger than the number of $ZZ \rightarrow 4$ leptons events.

Calculation of the signal is similar to that for the four lepton channel, with the change of one Z coupling from $g_{Z\ell\ell}$ to $g_{Z\nu\nu}$. There is no photon interference for the Z that decays to neutrinos. Since it is not possible to restrict the invariant mass of the neutrino pair to be in the vicinity of the Z resonance, one has to verify that the non-resonant Feynman diagrams ignored in our calculation do not significantly change the differential cross section. There are 10 Feynman diagrams contributing to $q\bar{q} \rightarrow \ell^+\ell^-\bar{\nu}_{\ell'}\nu_{\ell'}$, $\ell \neq \ell'$, and 19 contributing to $q\bar{q} \rightarrow \ell^+\ell^-\bar{\nu}_\ell\nu_\ell$ in the SM. The graphs of the $q\bar{q} \rightarrow W^+W^- \rightarrow \ell^+\ell^-\bar{\nu}_\ell\nu_\ell$ background, which is described in more detail below, are contained in this set. Using MADGRAPH [31] and the HELAS [32] library, we have calculated the SM cross section for $p\bar{p} \rightarrow e^+e^-\bar{\nu}\nu$ including the full set of contributing Feynman diagrams and summing over the three neutrino species. In Fig. 8 we compare the transverse momentum distribution of the e^+e^- system for $p\bar{p} \rightarrow e^+e^-\bar{\nu}\nu$ at the Tevatron resulting from the full set of tree level Feynman diagrams with the distribution obtained using the subset of diagrams contributing to $q\bar{q} \rightarrow ZZ \rightarrow e^+e^-\bar{\nu}\nu$ and $q\bar{q} \rightarrow W^+W^- \rightarrow e^+e^-\bar{\nu}_e\nu_e$ in the double pole approximation. Figure 8a displays the individual p_T distributions, whereas part b) of the figure shows the ratio of the differential

cross sections. In addition to the cuts listed in Sec. III A we have imposed a $\not{p}_T > 20$ GeV cut in Fig. 8. The non-resonant diagrams are seen to reduce (enhance) the rate by about 5% for $p_T(e^+e^-) < 80$ GeV ($p_T(e^+e^-) > 80$ GeV). This is significantly smaller than other theoretical uncertainties such as the factorization scale uncertainty in our calculation. In the following we shall therefore ignore effects of the non-resonant diagrams in channels where one of the Z bosons decays into neutrinos.

The most important background processes to $ZZ \rightarrow \ell^+\ell^-\bar{\nu}\nu$ production are $t\bar{t} \rightarrow W^+W^-\bar{b}b$, standard electroweak $W^+W^- + X$ production with $W^+W^- \rightarrow \ell^+\nu\ell^-\bar{\nu}$, and $Z(\rightarrow \ell^+\ell^-) + 1$ jet production with the jet rapidity outside the range covered by the detector, thus faking missing p_T . We will call this last process the “ $Z + 1$ jet” background. We have calculated the $t\bar{t}$ background using standard helicity amplitude techniques, fully including the subsequent decays $t \rightarrow Wb$ and $W \rightarrow \ell\nu$ and all decay correlations. Finite width effects for the top quarks and W ’s are included. Jets (partons) with $\Delta R(jj) < 0.4$ are merged into a single jet. We do not decay the bottom quarks explicitly, but do include a parameterized energy loss distribution to make a more realistic simulation of observed final state momenta and overall missing momentum. For $W^+W^- + X$ production we make use of the calculation described in Ref. [33]. For a realistic assessment of the $Z + 1$ jet background, a full-fledged Monte Carlo simulation is required. Here, for a first rough estimate, we use a simple parton level calculation. For a jet, i.e., a quark or gluon, to be misidentified as \not{p}_T at the Tevatron (LHC), we shall require that the jet pseudorapidity be $|\eta(j)| > 3.5$ ($|\eta(j)| > 5$).

Additional backgrounds originate from $b\bar{b}$ production and $Z \rightarrow \tau^+\tau^-$ decays. These backgrounds can be suppressed to a negligible level by requiring the angle in the transverse plane between a charged lepton and the missing transverse momentum to be between 20° and 160° , if $\not{p}_T < 50$ GeV.

Subsequently, in this section we shall focus on the $e^+e^-\not{p}_T$ final state. Virtually identical results are obtained for $ZZ \rightarrow \mu^+\mu^-\not{p}_T$. For reasons which will become clear shortly, we do not include a K -factor for the signal cross sections in the figures shown in this section. In addition to the cuts specified in Sec. III A, we impose a $\not{p}_T > 20$ GeV ($\not{p}_T > 50$ GeV) cut at the Tevatron (LHC), and the cut on the angle in the transverse plane between a charged lepton and the missing transverse momentum discussed above.

In Fig. 9a we show the transverse momentum distribution of the e^+e^- pair for $ZZ \rightarrow e^+e^-\not{p}_T$ in the SM (solid curve) and for $f_{40}^Z = 0.3$ (dashed line) at the Tevatron, together with the differential cross sections of the $t\bar{t}$ (dotted line), W^+W^- (dot-dashed line) and $Z + 1$ jet (long-dashed line) backgrounds. The cut on the angle in the transverse plane between a charged lepton and the missing transverse momentum is responsible for the slight dip in the ZZ differential cross section curves at $p_T(e^+e^-) \approx 50$ GeV in Fig. 9a.

One observes that all backgrounds shown in Fig. 9a are significantly larger than the ZZ signal at small values of $p_T(e^+e^-)$. Because of kinematical constraints, however, the $Z + 1$ jet background drops very rapidly with p_T . In a more complete treatment in which soft gluon and/or quark radiation and hadronization effects are included, one expects that the $p_T(e^+e^-)$ distribution will be somewhat harder for the $Z + 1$ jet background, especially at high transverse momentum. The $Z + 1$ jet background sensitively depends on the rapidity cut above which a jet is assumed to be misidentified as \not{p}_T . Our assumption that jets with $|\eta(j)| > 3.5$ will fake missing transverse momentum is probably conservative, and the $Z + 1$ jet background may well be significantly lower than shown in Fig. 9.

The W^+W^- background exceeds the ZZ signal cross section for $p_T(e^+e^-) < 80$ GeV. Since the tail of the $p_T(e^+e^-)$ distribution for W^+W^- production is very sensitive to NLL QCD corrections, we show the NLL $p_T(e^+e^-)$ distribution in Fig. 9a. The differential cross section of the $t\bar{t}$ background is larger than the SM signal for e^+e^- transverse momenta as large as 200 GeV, and may thus reduce the sensitivity to anomalous ZZV couplings. We do not show the distributions for the $b\bar{b}$ or $Z \rightarrow \tau^+\tau^-$ backgrounds, as they are negligible after the aforementioned angular cut.

The $t\bar{t}$ background can be virtually eliminated by requiring that no jets with $p_T(j) > 20$ GeV and $|\eta(j)| < 3.5$ are present. Such a jet veto also reduces the $W^+W^- + X$ background at large transverse momenta. This is shown in Fig. 9b. The remaining W^+W^- background will only marginally affect the sensitivity to ZZV couplings. The jet veto also significantly reduces the size of the NLL QCD corrections for the ZZ signal, justifying our procedure of not including a K -factor in the signal cross section in this section.

The $p_T(e^+e^-)$ distributions for signal and background processes at the LHC, requiring that no jets with $p_T(j) > 50$ GeV and $|\eta(j)| < 5$ are present, are shown in Fig. 10. Since the $t\bar{t}$ production cross section is more than two orders of magnitude larger than at the Tevatron, the $t\bar{t}$ background is significant even when a jet veto is required. For the cuts imposed, the $t\bar{t}$ background (dotted line) exceeds the signal for $p_T(e^+e^-) < 140$ GeV but is negligible for large transverse momenta. Both the W^+W^- and $t\bar{t}$ backgrounds could be reduced somewhat by choosing a smaller e^+e^- invariant mass window. Due to the more severe missing transverse momentum cut and the improved rapidity coverage of the hadronic calorimeters of the LHC experiments, the $Z + 1$ jet background is very small.

As in the $ZZ \rightarrow 4$ leptons channel, the $\Delta R(e^+e^-)$ and $\Delta\Phi(e^+e^-)$ distributions would be useful at the Tevatron in distinguishing between f_4^V and f_5^V , and in determining the sign of f_5^V . As shown in Fig. 11, the W^+W^- background is negligible in those regions of $\Delta R(e^+e^-)$ and $\Delta\Phi(e^+e^-)$ where the contributions from anomalous ZZV couplings are most pronounced. The jet veto imposed in Fig. 11 renders the $t\bar{t}$ background negligible (see Fig. 9b). The p_T cut removes events where the Z bosons are produced right at threshold and thus causes the peak in the $\Delta R(e^+e^-)$ ($\Delta\Phi(e^+e^-)$) distribution to shift from ≈ 3 (180°) to ≈ 2.6 ($\approx 140^\circ$). It has a similar effect on the $W^+W^- + 0$ jet background. Note that the W pair production background vanishes for $\Delta R(e^+e^-) < 1.4$ and $\Delta\Phi(e^+e^-) < 90^\circ$. The $Z + 1$ jet background is not shown in Fig. 11 to avoid overburdening the figure. Qualitatively, the $\Delta R(e^+e^-)$ and $\Delta\Phi(e^+e^-)$ distributions of the $Z + 1$ jet background are similar to those of the $W^+W^- + 0$ jet background.

For completeness, we show the $\Delta R(e^+e^-)$ and $\Delta\Phi(e^+e^-)$ distributions at the LHC in Fig. 12, imposing the same jet veto requirements as in Fig. 10. Due to the higher missing transverse momentum cut, the peak in the SM ZZ $\Delta R(e^+e^-)$ ($\Delta\Phi(e^+e^-)$) distribution is shifted to $\Delta R(e^+e^-) \approx 2$ ($\Delta\Phi(e^+e^-) \approx 100^\circ$). The $\Delta R(e^+e^-)$ distributions of the $t\bar{t}$ and $W^+W^- + 0$ jet background peak at similar values. Both backgrounds are negligible for $\Delta R(e^+e^-) < 1.4$. In the SM, the dominant W^\pm helicity at high energies in $u\bar{u} \rightarrow W^+W^-$ ($d\bar{d} \rightarrow W^+W^-$) is $\lambda_{W^\pm} = \mp 1$ ($\lambda_{W^\pm} = \pm 1$) [34]. Because of the $V - A$ nature of the $W\ell\nu$ coupling, the charged leptons in $W^+W^- \rightarrow e^+e^-\bar{\nu}_e\nu_e$ tend to be emitted either both into ($d\bar{d}$ annihilation), or both against the flight direction of their parent W boson ($u\bar{u}$ annihilation). If a jet veto is imposed, the W^+ and W^- in W pair production are almost back to back in the transverse plane, and so are the W decay leptons. The $\Delta\Phi(e^+e^-)$ distribution of the

$W^+W^- + 0$ jet background thus peaks at a significantly larger angle than that of the ZZ signal and of the $t\bar{t}$ background (see Fig. 12b). While the $t\bar{t}$ background is smaller than the SM ZZ signal for $\Delta\Phi(e^+e^-) < 50^\circ$, it is not negligible in this region.

D. The semi-hadronic channels

The decay modes where one of the two Z bosons decays hadronically have much larger branching fractions than the $ZZ \rightarrow 4$ leptons and the $ZZ \rightarrow \ell^+\ell^-\bar{\nu}\nu$ channels, but also much higher backgrounds. Nevertheless, these channels may be useful in searching for ZZV couplings: both CDF [3] and DØ [5] have successfully used the WW , $WZ \rightarrow \ell\nu jj$ channels to constrain anomalous WWV couplings in the past.

The main background sources are QCD $Z+2$ jet (“ Zjj ”) production and WZ production where the W decays hadronically into a pair of jets. In both cases the jet pair invariant mass is constrained to be near the Z pole, Eq. (14). The range of jj invariant masses considered here roughly corresponds to $M_Z \pm 2\sigma_{jj}$ where σ_{jj} is the two jet invariant mass resolution of the detector, which typically is $\sigma_{jj} = 5 - 9$ GeV [26,35]. The Z boson decays to either e^+e^- , $\mu^+\mu^-$ or invisibly to neutrinos.

The Zjj background consists of QCD real-emission corrections to Z production. These subprocesses include [36]

$$qg \rightarrow qg\ell^+\ell^-, \quad qq' \rightarrow qq'\ell^+\ell^-, \quad (15)$$

which are dominated by t -channel gluon exchange, and all crossing-related processes, such as

$$q\bar{q} \rightarrow g\ell^+\ell^-, \quad gg \rightarrow q\bar{q}\ell^+\ell^-. \quad (16)$$

Similar to the treatment of the signal processes, we use a parton-level Monte-Carlo program based on the work of Ref. [37] to model the QCD Zjj background. All interference effects between virtual photon and Z -exchange are included for charged lepton final states; for final state neutrino pairs there is no photon contribution. α_s running at one loop order is included, correcting the contribution from each phase space point from the input value of $\alpha_s(M_Z) = 0.118$. To compute the WZ background we make use of the calculation presented in Ref. [38].

Other potentially dangerous background sources are $t\bar{t}$ and Wjj production. The Wjj background contributes only to the $\bar{\nu}\nu jj$ final state. For $ZZ \rightarrow \ell^+\ell^-jj$, the $t\bar{t} \rightarrow \ell^+\nu_\ell\ell^-\bar{\nu}_\ell b\bar{b}$ background can be reduced by requiring that the missing transverse momentum is $\cancel{p}_T < 20$ GeV at the Tevatron, and $\cancel{p}_T < 40$ GeV at the LHC. The higher value for the LHC is motivated by pile-up effects due to the large number of interactions per beam crossing at the LHC design luminosity of $\mathcal{L} = 10^{34} \text{ cm}^{-2} \text{ s}^{-1}$. Pile-up effects amplify small momentum imbalance effects due to mismeasurements in the underlying event structure and can lead to a significant fake missing transverse momentum. Backgrounds from W^+W^-jj production are significantly smaller than those from $t\bar{t}$ production after imposing a \cancel{p}_T veto, and are ignored in the following.

For $ZZ \rightarrow \bar{\nu}\nu jj$, suppression of the $t\bar{t} \rightarrow \ell^+\nu_\ell\ell^-\bar{\nu}_\ell b\bar{b}$ and $W(\rightarrow \ell\nu)jj$ backgrounds is possible by requiring that there are no charged leptons with $p_T(\ell) > 10$ GeV and $|\eta(\ell)| < 2.5$

present in the event. The $t\bar{t} \rightarrow \ell\nu jj\bar{b}b$ background can be further reduced by imposing the constraint that the event does not contain more than two jets satisfying the p_T and pseudorapidity cuts described in Sec. III A. The Wjj background is calculated using the results of Ref. [37].

In the following, for $ZZ \rightarrow \ell^+\ell^-jj$, we shall sum over electrons and muons in the final state and impose a $\not{p}_T < 20$ GeV ($\not{p}_T < 40$ GeV) cut at the Tevatron (LHC) in addition to the charged lepton and jet p_T , pseudorapidity and invariant mass cuts specified in Sec. III A. For $ZZ \rightarrow \bar{\nu}\nu jj$, we require a missing transverse momentum of $\not{p}_T > 60$ GeV and no charged leptons with $p_T(\ell) > 10$ GeV and $|\eta(\ell)| < 2.5$. In addition, the number of jets which satisfy the cuts detailed in Sec. III A, n_j , has to be $n_j = 2$. The rather high \not{p}_T cut ensures that backgrounds from heavy quark production and three jet production, where the rapidity of one of the jets is outside the range covered by the detector, are sufficiently suppressed. At the LHC, a $\not{p}_T > 60$ GeV cut may well be too low to trigger on $jj\not{p}_T$ events, especially at high luminosities. However, since anomalous ZZV couplings lead to deviations only at large transverse momenta, raising the \not{p}_T cut to 100 GeV or even 200 GeV at the LHC will have very little impact on the sensitivity of the $ZZ \rightarrow \bar{\nu}\nu jj$ mode to ZZV couplings. Finally, all signal and background cross sections presented in this section are calculated at leading order.

The $p_T(\ell^+\ell^-)$ distribution for $ZZ \rightarrow \ell^+\ell^-jj$ is shown in Fig. 13a for the Tevatron, while Fig. 13b illustrates the Tevatron $p_T(jj)$ distribution for $\bar{\nu}\nu jj$ events. We display the SM cross section (solid line) together with the main backgrounds. We also show the ZZ cross section for $f_{40}^Z = 0.3$ (dashed line). The “kink” in the WZ and ZZ differential cross sections at $p_T \approx 250$ GeV is due to the $\Delta R(jj) > 0.6$ cut which becomes effective only at sufficiently high transverse momenta. Because of the missing transverse momentum (charged lepton) veto for $ZZ \rightarrow \ell^+\ell^-jj$ ($ZZ \rightarrow \bar{\nu}\nu jj$), the $t\bar{t}$ background is negligible at the Tevatron. The Wjj background, which contributes only to the $\bar{\nu}\nu jj$ final state, is considerably larger than the SM ZZ signal only for small values of $p_T(jj)$, thus it will not affect the sensitivity to anomalous couplings significantly. The WZ differential cross section (dotted line) is very similar to that of the SM signal over most of the p_T range considered, whereas the Zjj background dominates, overwhelming the signal even at very high transverse momenta. Its size is uniformly about one order of magnitude larger than the SM ZZ signal. It will therefore be very difficult to observe ZZ production in the semi-hadronic channels, if the SM prediction is correct. However, for sufficiently large anomalous ZZV couplings, the ZZ cross section exceeds the background at large transverse momenta. The semi-hadronic channels therefore may still be useful in obtaining limits on the ZZV couplings at the Tevatron.

The case is much worse for the LHC, as shown in Fig. 14. There the rate for Zjj events is almost two orders of magnitude greater than the SM signal, and approximately one order of magnitude greater than that for ZZ events for moderate values of f_{i0}^V ($i = 4, 5$). The Wjj background is a factor 3 to 10 larger than the SM $ZZ \rightarrow \bar{\nu}\nu jj$ signal. Although the $t\bar{t}$ background is significantly larger than at the Tevatron, it has almost no effect on the sensitivity of the $jj\not{p}_T$ final state to ZZV couplings.

It should be noted that NLL QCD corrections could worsen the signal to background ratio. QCD corrections enhance the ZZ signal cross section by about a factor 1.3 [29]. The full NLL QCD corrections to Zjj and Wjj production are currently not known. However, the QCD corrections to $Z\bar{b}b$ production in the limit of massless b -quarks increase the cross

section by about a factor 2 [39]. If the QCD corrections to Zjj and Wjj production are of similar size, they will weaken the signal to background ratio by about a factor 1.5.

In the ΔR and $\Delta\Phi$ distributions of the $\ell^+\ell^-$ system and the jet pair, the Zjj background overwhelms the ZZ signal even for rather large ZZV couplings. For the semi-hadronic ZZ final states it will therefore be very difficult to utilize these distributions in distinguishing the various neutral gauge boson couplings.

In our discussion of semi-hadronic final states in ZZ production, we have considered only inclusive jet rates. With the excellent b -tagging capabilities of the Tevatron [25,40] and LHC [26,41] experiments, one may also be able to search for anomalous ZZV couplings using $ZZ \rightarrow \ell^+\ell^-\bar{b}b$ and $ZZ \rightarrow \bar{\nu}\nu\bar{b}b$ decays. The $ZZ \rightarrow \ell^+\ell^-\bar{b}b$ ($ZZ \rightarrow \bar{\nu}\nu\bar{b}b$) cross section is about a factor 10 smaller than the $ZZ \rightarrow \ell^+\ell^-jj$ ($ZZ \rightarrow \bar{\nu}\nu jj$) rate if one requires that both b -quarks are tagged. The main backgrounds in these channels are $Z(\rightarrow \ell^+\ell^-)\bar{b}b$, $Z(\rightarrow \bar{\nu}\nu)\bar{b}b$ and $t\bar{t}$ production. The $Z\bar{b}b$ background is about a factor 3 larger than the $ZZ \rightarrow \ell^+\ell^-\bar{b}b$ and $ZZ \rightarrow \bar{\nu}\nu\bar{b}b$ signals [39]. The signal to background ratio thus is considerably better than in the $\ell^+\ell^-jj$ and $\bar{\nu}\nu jj$ cases. However, due to the smaller signal rate, one expects that the sensitivity limits obtained from $ZZ \rightarrow \ell^+\ell^-\bar{b}b$ ($ZZ \rightarrow \bar{\nu}\nu\bar{b}b$) will be about a factor 2 to 3 weaker than those derived from $ZZ \rightarrow \ell^+\ell^-jj$ ($ZZ \rightarrow \bar{\nu}\nu jj$).

IV. SENSITIVITY LIMITS

In this section we discuss the method to extract sensitivity bounds on anomalous couplings, and then determine the bounds on f_4^V and f_5^V which one expects to achieve with 2 fb^{-1} and 10 fb^{-1} of data at the Tevatron in Run II, and 10 fb^{-1} and 100 fb^{-1} at the LHC. For simplicity, we consider only real ZZV couplings.

We calculate 95% confidence level (CL) limits performing a χ^2 test. The statistical significance is calculated by splitting the selected p_T distribution into a number of bins, each with typically more than five events. We use the $p_T(\ell^+\ell^-)$ distribution for all final states except $\bar{\nu}\nu jj$ for which we use the $p_T(jj)$ differential cross section. Other distributions, such as the ZZ invariant mass distribution (useful only for $ZZ \rightarrow 4$ leptons), or the maximum or minimum transverse momenta of the charged leptons or jets, yield similar results. In deriving our sensitivity limits, we combine channels with electrons and muons in the final state. In each bin the Poisson statistics is approximated by a Gaussian distribution. Since we selected bins containing at least five events, the error introduced by this approximation is very small. The same method has been used in the past to estimate limits on anomalous $WW\gamma$ and $Z\gamma V$ couplings for Run I of the Tevatron [17,42]. The actual limits obtained from experimental data [2–7] agree well with the predicted bounds.

In order to derive realistic limits, we allow for a normalization uncertainty of 30% of the SM cross section. Backgrounds in the $ZZ \rightarrow \ell^+\ell^-\bar{\nu}\nu$, $ZZ \rightarrow \ell^+\ell^-jj$ and $ZZ \rightarrow \bar{\nu}\nu jj$ channels are included in our calculation. We impose the cuts described in detail in Sec. III A. In the $ZZ \rightarrow \ell^+\ell^-\bar{\nu}\nu$ case we assume that a jet veto has been imposed to reduce the $t\bar{t}$ background and require $p_T(\ell^+\ell^-) > 40 \text{ GeV}$ to eliminate the Zj background. For $ZZ \rightarrow \ell^+\ell^-jj$ we require that events do not contain missing transverse momentum of more than 20 GeV (40 GeV) at the Tevatron (LHC). Finally, for $ZZ \rightarrow \bar{\nu}\nu jj$ we impose a charged lepton veto ($p_T(\ell) < 10 \text{ GeV}$ if $|\eta(\ell)| < 2.5$) and require exactly two jets to reduce the Wjj

and $t\bar{t}$ backgrounds. As before, we use a form factor of the form of Eq. (2) with $n = 3$ and $\Lambda_{FF} = 750$ GeV ($\Lambda_{FF} = 2$ TeV) for the Tevatron (LHC).

Non-negligible interference effects between the various ZZV couplings are found only between f_4^Z and f_4^γ , and between f_5^Z and f_5^γ . The f_4^V and f_5^V couplings do not interfere, as expected from the CP-odd nature of f_4^V and CP-even nature of f_5^V . This result is demonstrated in Fig. 15, where we show the 1σ and 2σ limit contours for $ZZ \rightarrow \ell^+\ell^-\bar{\nu}\nu$ events in 2 fb^{-1} of data at the Tevatron Run II. In each graph, only those couplings plotted against each other are assumed to be different from their SM values. Plots similar to those shown in Fig. 15 can be obtained for the LHC, other final states, and different values of Λ_{FF} . As a result of the correlations between f_4^Z and f_4^γ , and between f_5^Z and f_5^γ , different anomalous coupling contributions to the helicity amplitudes may cancel partially, resulting in weaker bounds than if only one coupling at a time is allowed to deviate from its SM value.

In Table I we display 95% confidence level (CL) sensitivity limits expected from the Tevatron Run II for integrated luminosities of 2 fb^{-1} and 10 fb^{-1} , taking into account the correlations between different anomalous couplings. Due to the small branching ratio for $p\bar{p} \rightarrow ZZ \rightarrow 4$ leptons, the number of expected events in that channel for 2 fb^{-1} is too low to allow for an analysis of the $p_T(\ell^+\ell^-)$ distribution using the method chosen here. The bounds obtained from $ZZ \rightarrow \ell^+\ell^-\bar{\nu}\nu$ and $ZZ \rightarrow \bar{\nu}\nu jj$ are quite similar. The cross section for $ZZ \rightarrow \bar{\nu}\nu jj$ is about a factor 10 larger than that for $ZZ \rightarrow \ell^+\ell^-\bar{\nu}\nu$; however, the large background from Zjj production considerably limits the sensitivity to ZZV couplings for $ZZ \rightarrow \bar{\nu}\nu jj$. The limits from the $ZZ \rightarrow \ell^+\ell^-jj$ and $ZZ \rightarrow 4$ leptons channels are about a factor 1.5 and 2 weaker than those from $ZZ \rightarrow \ell^+\ell^-\bar{\nu}\nu$ and $ZZ \rightarrow \bar{\nu}\nu jj$. We do not attempt to combine limits from different channels. From Table I it is clear that this could result in a significant improvement of the bounds.

In Table II we display 95% CL sensitivity limits expected from the LHC for integrated luminosities of 10 fb^{-1} and 100 fb^{-1} . The most stringent bounds are obtained from the $ZZ \rightarrow \ell^+\ell^-\bar{\nu}\nu$ channel. The $ZZ \rightarrow 4$ leptons channel yields sensitivity limits which are a factor 1.6 to 2 weaker; while, due to the increased Zjj and Wjj backgrounds, the limits which can be achieved from analyzing the semi-hadronic channels are a factor 2.5 to 4 worse than those found for $ZZ \rightarrow \ell^+\ell^-\bar{\nu}\nu$.

The sensitivity bounds on the ZZZ couplings at the Tevatron (LHC) are up to 10% (20%) better than those on the corresponding $ZZ\gamma$ couplings. The sensitivities achievable for an integrated luminosity of 10 fb^{-1} at the Tevatron are about a factor 1.5 to 1.7 more stringent than those found with 2 fb^{-1} . At the LHC, increasing the integrated luminosity by a factor 10 improves the limits by approximately a factor 2. These numbers are in good agreement with the naive scaling law which predicts that sensitivity limits on anomalous couplings improve roughly with $(\int \mathcal{L} dt)^{1/4}$ [35]. Due to interference with the SM helicity amplitudes, the limits on f_{50}^V are somewhat sign dependent. In contrast, because of their CP-violating nature, contributions to the helicity amplitudes proportional to f_{40}^V do not interfere with the SM terms, and the bounds on these couplings do not depend on the sign of the coupling.

The W^+W^- and $t\bar{t}$ backgrounds only marginally influence the sensitivity limits obtained in the $ZZ \rightarrow \ell^+\ell^-\bar{\nu}\nu$ case. The limits derived from $ZZ \rightarrow \ell^+\ell^-jj$ and $ZZ \rightarrow \bar{\nu}\nu jj$ production, on the other hand, are significantly degraded by the Zjj and Wjj backgrounds and thus depend on an accurate knowledge of the signal to background ratio. The signal

to background ratio is affected by QCD corrections which are not yet fully known, by the factorization scale uncertainty, and by uncertainties originating from the parton distribution functions. Changing the signal to background ratio by a factor 1.5 alters the sensitivity limits by 10 – 15%.

The sensitivity limits depend significantly on the scale Λ_{FF} . For example, at the Tevatron, increasing (decreasing) the form factor scale to $\Lambda_{FF} = 1000$ GeV ($\Lambda_{FF} = 500$ GeV) improves (weakens) the bounds which can be achieved by a factor 1.5 (2). To a lesser degree, the limits also depend on the power n in the form factor, which we have assumed to be $n = 3$. A smaller value of n allows for additional high p_T events and therefore leads to a somewhat increased sensitivity to the low energy values of the ZZV couplings.

Limits on the anomalous couplings depend on the power, n , and the scale, Λ_{FF} , of the form factor. These parameters are *a priori* unknown, as they represent our ignorance of the scale and the nature of new physics beyond the SM. In Ref. [11] it was pointed out that in final states without missing transverse momentum one can in principle determine the form factor by fitting the \sqrt{s} distribution simultaneously to f_{i0}^V , Λ_{FF} and n . However, a study [43] carried out for $WW\gamma$ couplings demonstrated that the method will not produce competitive limits. One expects that a similar result is obtained for ZZV couplings. Alternatively, if non-zero anomalous couplings are observed, the method may be useful in determining the shape of the form factor which provides indirect information on the dynamics of the underlying new physics.

V. SUMMARY AND CONCLUSIONS

ZZ production in hadronic collisions provides an opportunity to probe neutral gauge boson self-interactions in a direct way. In this paper we presented a detailed investigation of how well future experiments at the Tevatron and LHC will be able to measure the ZZV couplings. Our calculation has been carried out in the double pole approximation, using the most general ZZV vertex function which respects Lorentz and electromagnetic gauge invariance. If both Z bosons are on-shell, there are two independent ZZZ (f_4^Z and f_5^Z) and two $ZZ\gamma$ couplings (f_4^γ and f_5^γ). Z decays with full decay correlations and finite Z width effects are included in our calculation. Non-resonant Feynman diagrams, except for time-like photon exchange diagrams, and contributions from $gg \rightarrow ZZ$ are not taken into account. The non-resonant Feynman diagrams change the differential cross section by at most 5%. The contribution from gluon fusion enhances the cross section by about 1% (15%) at the Tevatron (LHC). NLL QCD corrections are approximated in our calculation where appropriate by a simple K -factor.

S -matrix unitarity requires that the ZZV couplings are momentum dependent form factors. We derived constraints on the low energy values of the ZZV form factors and the shape of the form factor from a partial wave analysis of the inelastic ZZ production amplitude in fermion antifermion annihilation (see Eqs. (10) and (11)).

The effects of anomalous ZZV couplings are enhanced at large energies. They lead to a broad increase in the ZZ invariant mass distribution and in various transverse momentum distributions. We considered four signatures of ZZ production: $ZZ \rightarrow 4$ leptons, $ZZ \rightarrow \ell^+\ell^-\bar{\nu}\nu$, $ZZ \rightarrow \ell^+\ell^-jj$, and $ZZ \rightarrow \bar{\nu}\nu jj$. The $ZZ \rightarrow 4$ leptons channel is almost background free but suffers from a small event rate due to the small branching ratio for a Z pair decaying

into four charged leptons. The rate for $ZZ \rightarrow \ell^+\ell^-\bar{\nu}\nu$ is approximately a factor six larger than that for $ZZ \rightarrow 4$ leptons; however, W^+W^- and $t\bar{t}$ production constitute non-negligible backgrounds at small values of $p_T(\ell^+\ell^-)$. The $ZZ \rightarrow \ell^+\ell^-jj$ and $ZZ \rightarrow \bar{\nu}\nu jj$ modes have larger branching ratios than the $ZZ \rightarrow 4$ leptons and $ZZ \rightarrow \ell^+\ell^-\bar{\nu}\nu$ channels, but also much higher backgrounds. The main background source for the semi-hadronic final states is QCD $Z + 2$ jet production. The $Z + 2$ jet cross section is about a factor 20 (50) larger than the ZZ signal at the Tevatron (LHC). Nevertheless, we found that these channels may be useful in searching for ZZV couplings.

All ZZV couplings have similar high energy behavior. This makes it difficult to distinguish the various ZZV couplings in the transverse momentum and ZZ invariant mass distributions. We found that in the $ZZ \rightarrow 4$ leptons and $ZZ \rightarrow \ell^+\ell^-\bar{\nu}\nu$ channels, the distributions of the lego plot separation, $\Delta R(\ell^+\ell^-)$, and the angle in the transverse plane between the charged leptons, $\Delta\Phi(\ell^+\ell^-)$, may be useful to distinguish f_4^V from f_5^V and to determine the sign of f_5^V . Since f_4^V violate CP conservation, terms in the helicity amplitudes proportional to f_4^V do not interfere with the SM helicity amplitudes, thus it is impossible to determine the sign of f_4^V using the $\Delta R(\ell^+\ell^-)$ and $\Delta\Phi(\ell^+\ell^-)$ distributions. In the semi-hadronic modes, the ZZ signal is overwhelmed by the Zjj background in these distributions, even for rather large anomalous couplings. Unfortunately, the two distributions will not be useful in distinguishing between f_i^Z and f_i^γ as they differ very little in shape for ZZZ and $ZZ\gamma$ couplings.

In order to determine the bounds on the ZZV couplings which one can hope to achieve in future Tevatron and LHC experiments, we have performed a χ^2 test for the four different final states, using the $\ell^+\ell^-$ and dijet transverse momentum distributions. At the Tevatron, with an integrated luminosity of 2 fb^{-1} , one will be able to measure f_4^V and f_5^V with a precision of $15 - 20\%$ (95% CL) in the $ZZ \rightarrow \ell^+\ell^-\bar{\nu}\nu$ and $ZZ \rightarrow \bar{\nu}\nu jj$ channels for a form factor scale of $\Lambda_{FF} = 750 \text{ GeV}$. The limits obtained from the $ZZ \rightarrow 4$ leptons and $ZZ \rightarrow \ell^+\ell^-jj$ channels are about a factor 2 and 1.5 weaker than those which can be achieved in the other two channels (see Table I). At the LHC with 100 fb^{-1} , the ZZV couplings can be measured with an accuracy of $3 \times 10^{-3} - 4 \times 10^{-3}$ (95% CL) in $pp \rightarrow ZZ \rightarrow \ell^+\ell^-\bar{\nu}\nu$ for $\Lambda_{FF} = 2 \text{ TeV}$. The limits obtained from the other three channels are a factor 1.6 to 4 weaker (see Table II).

The sensitivity limits which can be achieved at the Tevatron in Run II and the LHC should be compared with the bounds from recent measurements at LEP2 and expectations for a future linear collider, as well as predictions from theory. The combined 95% CL limits from the LEP2 experiments presently are [44]

$$-0.66 < f_4^Z < 0.68, \quad -0.40 < f_4^\gamma < 0.38, \quad (17)$$

$$-1.06 < f_5^Z < 0.69, \quad -0.89 < f_5^\gamma < 0.86. \quad (18)$$

It should be noted that the LEP2 limits do not contain any form factor effects. For the form and scale chosen here, these effects weaken the limits by about 20%. In Run II, CDF and DØ will be able to improve these bounds by at least a factor 3 to 6. At a e^+e^- Linear Collider (LC) with $\sqrt{s} = 500 \text{ GeV}$ and an integrated luminosity of $\int \mathcal{L} dt = 100 \text{ fb}^{-1}$, one expects to measure the ZZV couplings with a precision of [45] $4 \times 10^{-3} - 6 \times 10^{-3}$ (95% CL). This is comparable to the bounds which one hopes to achieve at the LHC. One loop corrections in the SM, in supersymmetric models, and in models with heavy fermions, induce ZZV couplings which are of $\mathcal{O}(10^{-4})$ or less.

In view of our present poor knowledge of the ZZV couplings, the direct measurement of these couplings in Run II and at the LHC will constitute major progress. However, it will be very difficult to achieve a precision which will make it possible to test the SM one loop prediction for the ZZV couplings.

ACKNOWLEDGMENTS

We would like to thank S. Dasu, D. Denegri and J. Womersley for useful and stimulating discussions. One of us (UB) would like to thank the Fermilab Theory Group, where part of this work was carried out, for its generous hospitality. This work has been supported in part by Department of Energy contract No. DE-AC02-76CH03000 and NSF grant PHY-9970703.

REFERENCES

- [1] G. Bella *et al.* (The LEP TGC Working Group), LEPEWWG/TGC/2000-01 (March 2000) and references therein.
- [2] F. Abe *et al.* (CDF Collaboration), Phys. Rev. Lett. **74**, 1936 (1995) and Phys. Rev. Lett. **78**, 4537 (1997).
- [3] F. Abe *et al.* (CDF Collaboration), Phys. Rev. Lett. **75**, 1017 (1995).
- [4] S. Abachi *et al.* (DØ Collaboration), Phys. Rev. Lett. **75**, 1034 (1995); Phys. Rev. Lett. **78**, 3634 (1997) and Phys. Rev. Lett. **75**, 1023 (1995); B. Abbott *et al.* (DØ Collaboration), Phys. Rev. **D58**, 051101 (1998), and Phys. Rev. **D58**, 031102 (1998).
- [5] S. Abachi *et al.* (DØ Collaboration), Phys. Rev. Lett. **77**, 3303 (1996); B. Abbott *et al.* (DØ Collaboration), Phys. Rev. Lett. **79**, 1441 (1997); hep-ex/9912033, to appear in Phys. Rev. **D**, and Phys. Rev. **D60**, 072002 (1999).
- [6] F. Abe *et al.* (CDF Collaboration), Phys. Rev. Lett. **74**, 1941 (1995).
- [7] S. Abachi *et al.* (DØ Collaboration), Phys. Rev. Lett. **75**, 1028 (1995); Phys. Rev. Lett. **78**, 3640 (1997); B. Abbott *et al.* (DØ Collaboration), Phys. Rev. **D57**, 3817 (1998).
- [8] B. Ashmanskas, talk given at the “Les Rencontres de Physique de la Vallée d’Aoste”, 26 February – 4 March 2000, La Thuile, Vallée d’Aoste, Italy.
- [9] The LHC Study Group, Design Study of the Large Hadron Collider, CERN 91-03, 1991; L. R. Evans, Proceedings of the “27th International Conference on High Energy Physics”, Glasgow, Scotland, July 1994, Vol. II, p. 1417 and CERN-AC-95-002 (preprint, June 1995).
- [10] F. Boudjema, N. Dombey, and M. Krawczyk, Phys. Lett. **B222**, 507 (1989).
- [11] G.J. Gounaris, J.Layssac and F.M. Renard, Phys. Rev. **D61**, 073013 (2000).
- [12] K. Hagiwara, R. D. Peccei, D. Zeppenfeld and K. Hikasa, Nucl. Phys. **B282**, 253 (1987).
- [13] A. Barroso, F. Boudjema, J. Cole and N. Dombey, Z. Phys. **C28**, 149 (1985); F. Boudjema and C. Hamzaoui, Phys. Rev. **D43**, 3748 (1991).
- [14] G.J. Gounaris, J.Layssac and F.M. Renard, hep-ph/0003143 (March 2000).
- [15] G.J. Gounaris, J.Layssac and F.M. Renard, hep-ph/0005269 (May 2000).
- [16] J. M. Cornwall, D. N. Levin and G. Tiktopoulos, Phys. Rev. Lett. **30**, 1268 (1973); Phys. Rev. **D10**, 1145 (1974); C. H. Llewellyn Smith, Phys. Lett. **B46**, 233 (1973); S. D. Joglekar, Ann. of Phys. **83**, 427 (1974).
- [17] U. Baur and E.L. Berger, Phys. Rev. **D47**, 4889 (1993).
- [18] U. Baur and D. Zeppenfeld, Phys. Lett. **B201**, 383 (1988).
- [19] D.E. Groom *et al.* (Particle Data Group), Eur. Phys. J. **C15**, 1 (2000).
- [20] D. Chang, W.Y. Keung, and P.B. Pal, Phys. Rev. **D51**, 1326 (1995).
- [21] K. Hagiwara and D. Zeppenfeld, Nucl. Phys. **B274**, 1 (1986).
- [22] E.W.N. Glover and J.J. van der Bij, Nucl. Phys. **B321**, 561 (1989).
- [23] D. Abbaneo *et al.* (The LEP Electroweak Working Group), CERN-EP-2000-016 (January 2000).
- [24] H.L. Lai *et al.*, Phys. Rev. **D55**, 1280 (1997).
- [25] F. Abe *et al.* (CDF Collaboration), FERMILAB-Pub-96/390-E, (report, October 1996).
- [26] A. Airapetian *et al.* (ATLAS Collaboration), “ATLAS Detector and Physics Performance Technical Design Report, Vol. 2”, CERN-LHCC-99-15, (report, May 1999).
- [27] F. Abe *et al.* (CDF Collaboration), Phys. Rev. Lett. **76**, 3070 (1996) and Phys. Rev. **D52**, 2624 (1995).

- [28] B. Abbott *et al.* (DØ Collaboration), Phys. Rev. **D60**, 052003 (1999).
- [29] B. Mele, P. Nason and G. Ridolfi, Nucl. Phys. **B357**, 409 (1991); J. Ohnemus and J. Owens, Phys. Rev. **D43**, 3626 (1991); L. Dixon, Z. Kunszt, and A. Signer, Phys. Rev. **D60**, 114037 (1999); J.M. Campbell and R.K. Ellis, Phys. Rev. **D60**, 113006 (1999).
- [30] M.J. Duncan, Phys. Lett. **B179**, 393 (1986); T. Matsuura and J.J. van der Bij, Z. Phys. **C51**, 259 (1991).
- [31] T. Stelzer and W.F. Long, Comput. Phys. Commun. **81**, 357 (1994).
- [32] H. Murayama, I. Watanabe and K. Hagiwara, KEK report KEK-91-1 (January 1992).
- [33] U. Baur, T. Han and J. Ohnemus, Phys. Rev. **D53**, 1098 (1996).
- [34] K. Hagiwara, R. D. Peccei, D. Zeppenfeld and K. Hikasa, Nucl. Phys. **B282**, 253 (1987); J. Stroughair and C. L. Bilchak, Z. Phys. **C23**, 377 (1984); C. L. Bilchak, R. W. Brown and J. D. Stroughair, Phys. Rev. **D29**, 375 (1984).
- [35] U. Baur *et al.*, hep-ph/0005226, to appear in the Proceedings of the “Fermilab Run II Workshop on QCD and Weak Boson Physics”, Fermilab, 1999.
- [36] S. D. Ellis, R. Kleiss, and W. J. Stirling, Phys. Lett. **B154**, 435 (1985); R. Kleiss and W. J. Stirling, Nucl. Phys. **B262**, 235 (1985); Phys. Lett. **B180**, 171 (1986); J. F. Gunion, Z. Kunszt, and M. Soldate, Phys. Lett. **B163**, 389 (1985); Erratum, Phys. Lett. **B168**, 427 (1986); J. F. Gunion and M. Soldate, Phys. Rev. **D34**, 826 (1986); R. K. Ellis and R. J. Gonsalves, in “Proc. of the Workshop on Super High Energy Physics”, Eugene, Oregon (1985), ed. D. E. Soper, p. 287.
- [37] V. Barger, T. Han, J. Ohnemus and D. Zeppenfeld, Phys. Rev. Lett. **62**, 1971 (1989) and Phys. Rev. **D40**, 2888 (1989).
- [38] V. Barger, T. Han, J. Ohnemus and D. Zeppenfeld, Phys. Rev. **D41**, 2782 (1990).
- [39] J. Campbell and R.K. Ellis, Fermilab-Pub-00/145-T (June 2000).
- [40] S. Abachi *et al.*, (DØ Collaboration), Fermilab-Pub-96/357-E, 1996.
- [41] M. Beneke *et al.*, hep-ph/0003033, Proceedings of the “1999 CERN Workshop on Standard Model Physics (and more) at the LHC”, CERN Yellow Report CERN-2000-004, eds. G. Altarelli and M. Mangano.
- [42] U. Baur and E. L. Berger, Phys. Rev. **D41**, 1476 (1990).
- [43] S. Haywood *et al.*, hep-ph/0003275, Proceedings of the “1999 CERN Workshop on Standard Model Physics (and more) at the LHC”, CERN Yellow Report CERN-2000-004, eds. G. Altarelli and M. Mangano.
- [44] C. Matteuzzi, talk given at the “XXXth International Conference on High Energy Physics”, Osaka, Japan, July 27 – August 2, 2000.
- [45] S. Rosati, talk given at the Linear Collider Workshop, Padova, Italy, May 2000.

TABLES

TABLE I. Sensitivities achievable at 95% CL for anomalous ZZV couplings in $p\bar{p} \rightarrow ZZ \rightarrow 4$ leptons, $p\bar{p} \rightarrow ZZ \rightarrow \ell^+\ell^-\bar{\nu}\nu$, $p\bar{p} \rightarrow ZZ \rightarrow \ell^+\ell^-jj$, and $p\bar{p} \rightarrow ZZ \rightarrow \bar{\nu}\nu jj$ at the Tevatron ($\sqrt{s} = 2$ TeV) for an integrated luminosity of (a) 2 fb^{-1} , and (b) 10 fb^{-1} . The limits for each coupling apply for arbitrary values of the other couplings. For the form factor we use the form of Eq. (2) with $n = 3$ and $\Lambda_{FF} = 750$ GeV. The cuts imposed are discussed in the text.

(a) $\int \mathcal{L} dt = 2 \text{ fb}^{-1}$				
coupling	$ZZ \rightarrow 4 \text{ leptons}$	$ZZ \rightarrow \ell^+\ell^-\bar{\nu}\nu$	$ZZ \rightarrow \ell^+\ell^-jj$	$ZZ \rightarrow \bar{\nu}\nu jj$
f_{40}^Z	–	+0.169 –0.169	+0.219 –0.218	+0.159 –0.160
f_{40}^γ	–	+0.175 –0.174	+0.222 –0.221	+0.163 –0.162
f_{50}^Z	–	+0.171 –0.204	+0.220 –0.244	+0.162 –0.184
f_{50}^γ	–	+0.184 –0.202	+0.229 –0.241	+0.170 –0.179
(b) $\int \mathcal{L} dt = 10 \text{ fb}^{-1}$				
coupling	$ZZ \rightarrow 4 \text{ leptons}$	$ZZ \rightarrow \ell^+\ell^-\bar{\nu}\nu$	$ZZ \rightarrow \ell^+\ell^-jj$	$ZZ \rightarrow \bar{\nu}\nu jj$
f_{40}^Z	+0.180 –0.179	+0.097 –0.097	+0.146 –0.145	+0.106 –0.106
f_{40}^γ	+0.185 –0.185	+0.100 –0.099	+0.148 –0.147	+0.109 –0.108
f_{50}^Z	+0.178 –0.216	+0.092 –0.120	+0.144 –0.167	+0.105 –0.127
f_{50}^γ	+0.192 –0.213	+0.103 –0.115	+0.151 –0.163	+0.112 –0.121

TABLE II. Sensitivities achievable at 95% CL for anomalous ZZV couplings in $pp \rightarrow ZZ \rightarrow 4$ leptons, $pp \rightarrow ZZ \rightarrow \ell^+\ell^-\bar{\nu}\nu$, $pp \rightarrow ZZ \rightarrow \ell^+\ell^-jj$, and $pp \rightarrow ZZ \rightarrow \bar{\nu}\nu jj$ at the LHC ($\sqrt{s} = 14$ TeV) for an integrated luminosity of (a) 10 fb^{-1} , and (b) 100 fb^{-1} . The limits for each coupling apply for arbitrary values of the other couplings. For the form factor we use the form of Eq. (2) with $n = 3$ and $\Lambda_{FF} = 2$ TeV. The cuts imposed are discussed in the text.

(a) $\int \mathcal{L} dt = 10 \text{ fb}^{-1}$				
coupling	$ZZ \rightarrow 4 \text{ leptons}$	$ZZ \rightarrow \ell^+\ell^-\bar{\nu}\nu$	$ZZ \rightarrow \ell^+\ell^-jj$	$ZZ \rightarrow \bar{\nu}\nu jj$
f_{40}^Z	+0.0115	+0.0060	+0.0230	+0.0156
	-0.0114	-0.0060	-0.0228	-0.0154
f_{40}^γ	+0.0139	+0.0072	+0.0274	+0.0186
	-0.0139	-0.0072	-0.0274	-0.0186
f_{50}^Z	+0.0119	+0.0062	+0.0226	+0.0160
	-0.0113	-0.0060	-0.0220	-0.0158
f_{50}^γ	+0.0137	+0.0072	+0.0268	+0.0188
	-0.0145	-0.0075	-0.0274	-0.0190
(b) $\int \mathcal{L} dt = 100 \text{ fb}^{-1}$				
coupling	$ZZ \rightarrow 4 \text{ leptons}$	$ZZ \rightarrow \ell^+\ell^-\bar{\nu}\nu$	$ZZ \rightarrow \ell^+\ell^-jj$	$ZZ \rightarrow \bar{\nu}\nu jj$
f_{40}^Z	+0.0052	+0.0031	+0.0130	+0.0088
	-0.0051	-0.0031	-0.0128	-0.0086
f_{40}^γ	+0.0062	+0.0038	+0.0154	+0.0104
	-0.0062	-0.0038	-0.0154	-0.0104
f_{50}^Z	+0.0053	+0.0032	+0.0128	+0.0092
	-0.0051	-0.0031	-0.0122	-0.0088
f_{50}^γ	+0.0061	+0.0037	+0.0148	+0.0104
	-0.0065	-0.0039	-0.0154	-0.0108

FIGURES

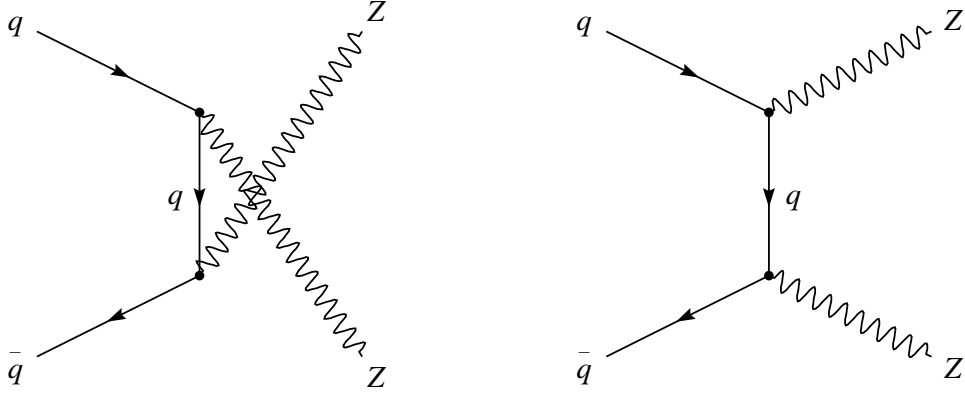


FIG. 1. The Feynman diagrams for the tree level processes contributing to $p\bar{p} \rightarrow ZZ$ in the SM.

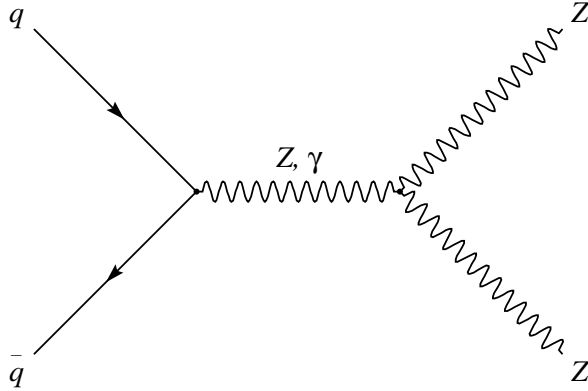


FIG. 2. Contributions of ZZZ and $ZZ\gamma$ diagrams to $q\bar{q} \rightarrow ZZ$.

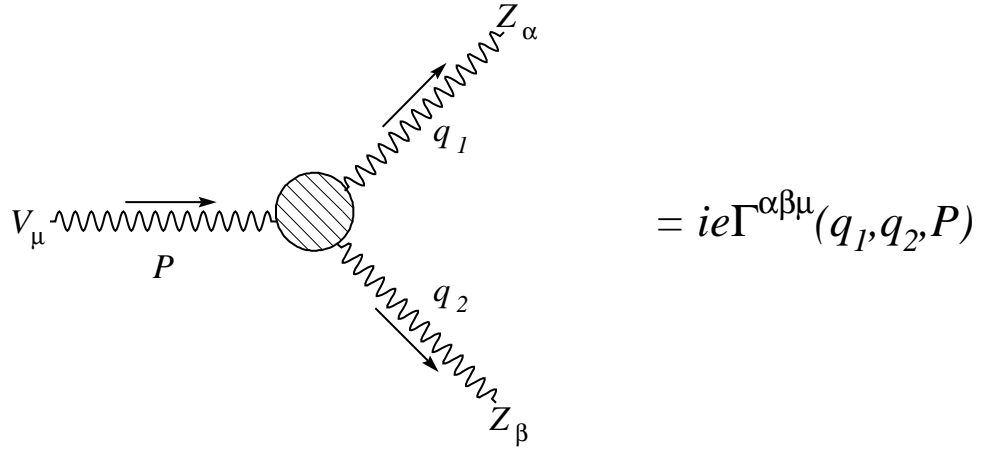


FIG. 3. Feynman rule for the general ZZV ($V = Z, \gamma$) vertex. The vertex function is given in Eq. (1). e is the charge of the proton.

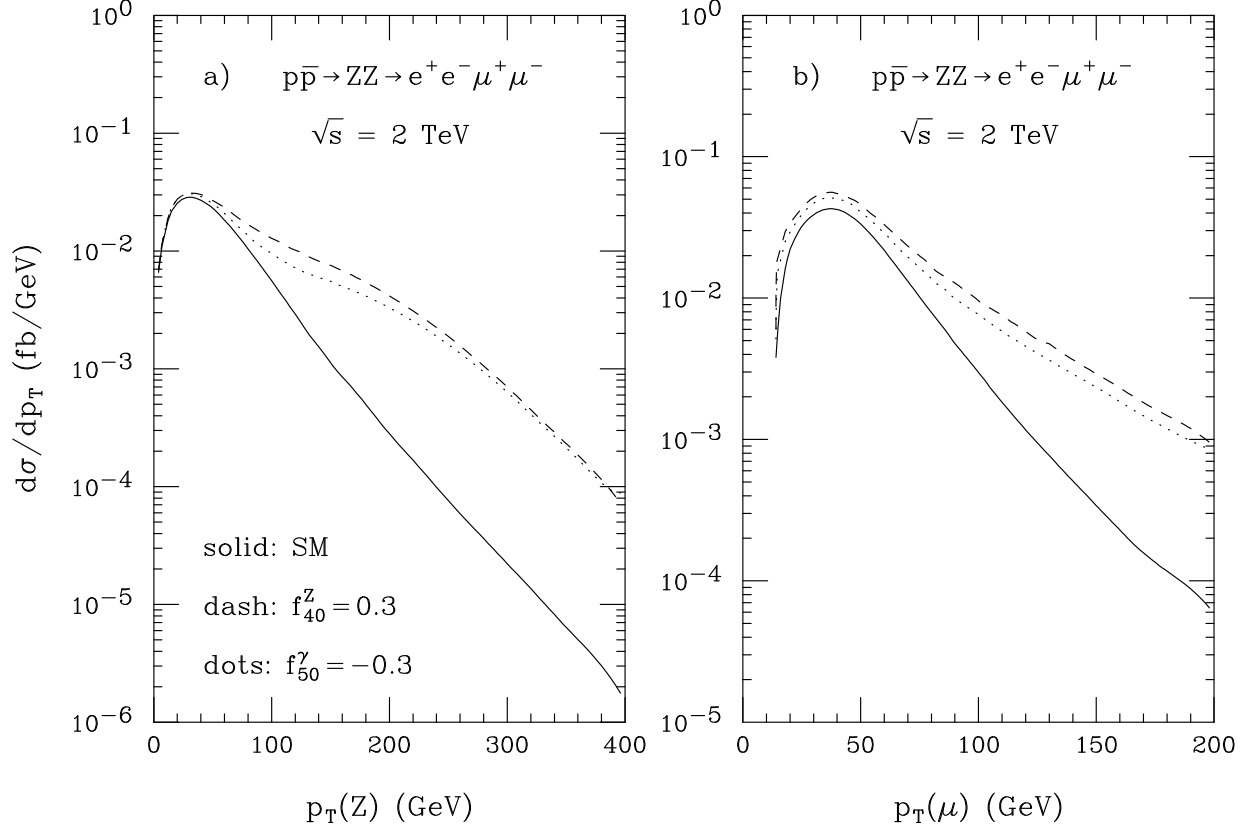


FIG. 4. The $p_T(Z)$ and $p_T(\mu)$ distributions in $p\bar{p} \rightarrow ZZ \rightarrow e^+e^-\mu^+\mu^-$ at the Tevatron ($\sqrt{s} = 2 \text{ TeV}$) in the SM (solid line), for $f_{40}^Z = 0.3$, and $f_{50}^\gamma = -0.3$. The cuts imposed are described in detail in Sec. III A. The form factor scale has been set to $\Lambda_{FF} = 750 \text{ GeV}$.

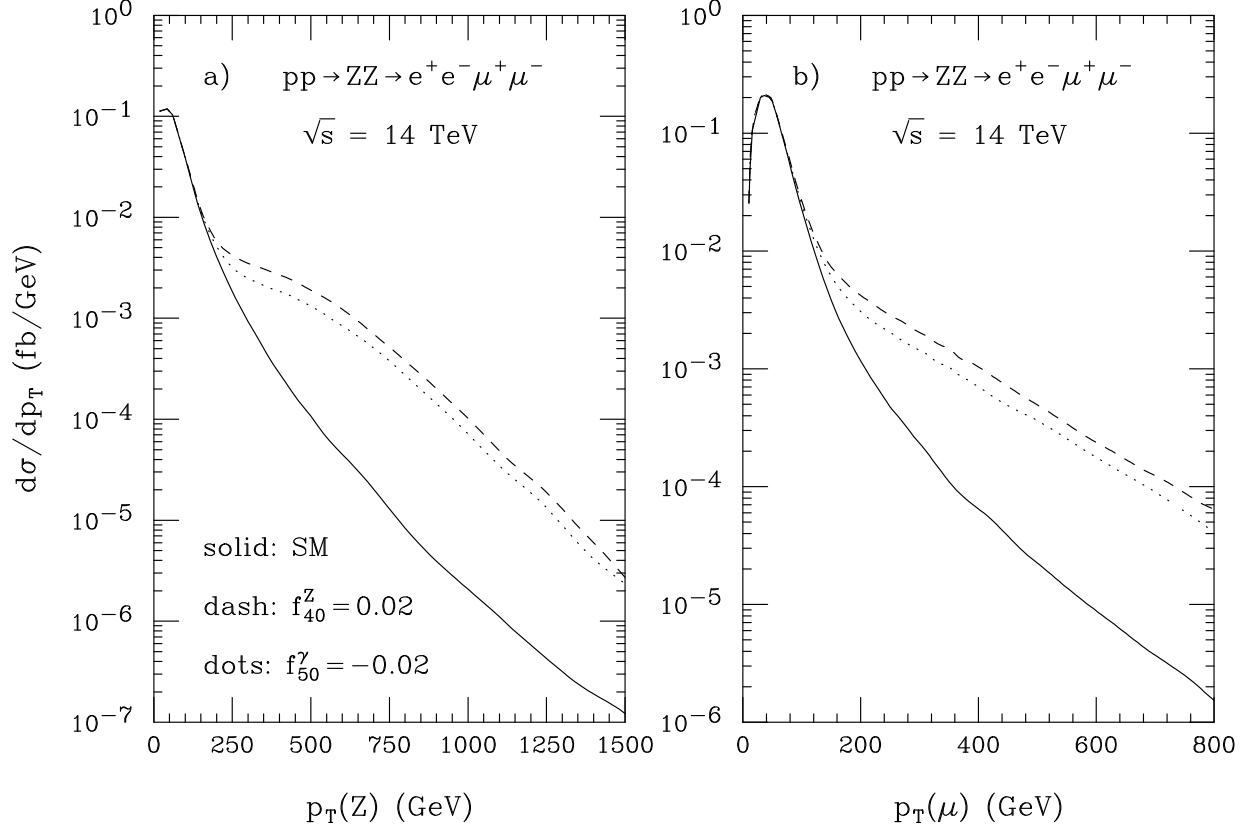


FIG. 5. The $p_T(Z)$ and $p_T(\mu)$ distributions in $pp \rightarrow ZZ \rightarrow e^+e^-\mu^+\mu^-$ at the LHC ($\sqrt{s} = 14 \text{ TeV}$) in the SM (solid line), for $f_{40}^Z = 0.02$, and $f_{50}^\gamma = -0.02$. The cuts imposed are described in detail in Sec. III A. The form factor scale has been set to $\Lambda_{FF} = 2 \text{ TeV}$.

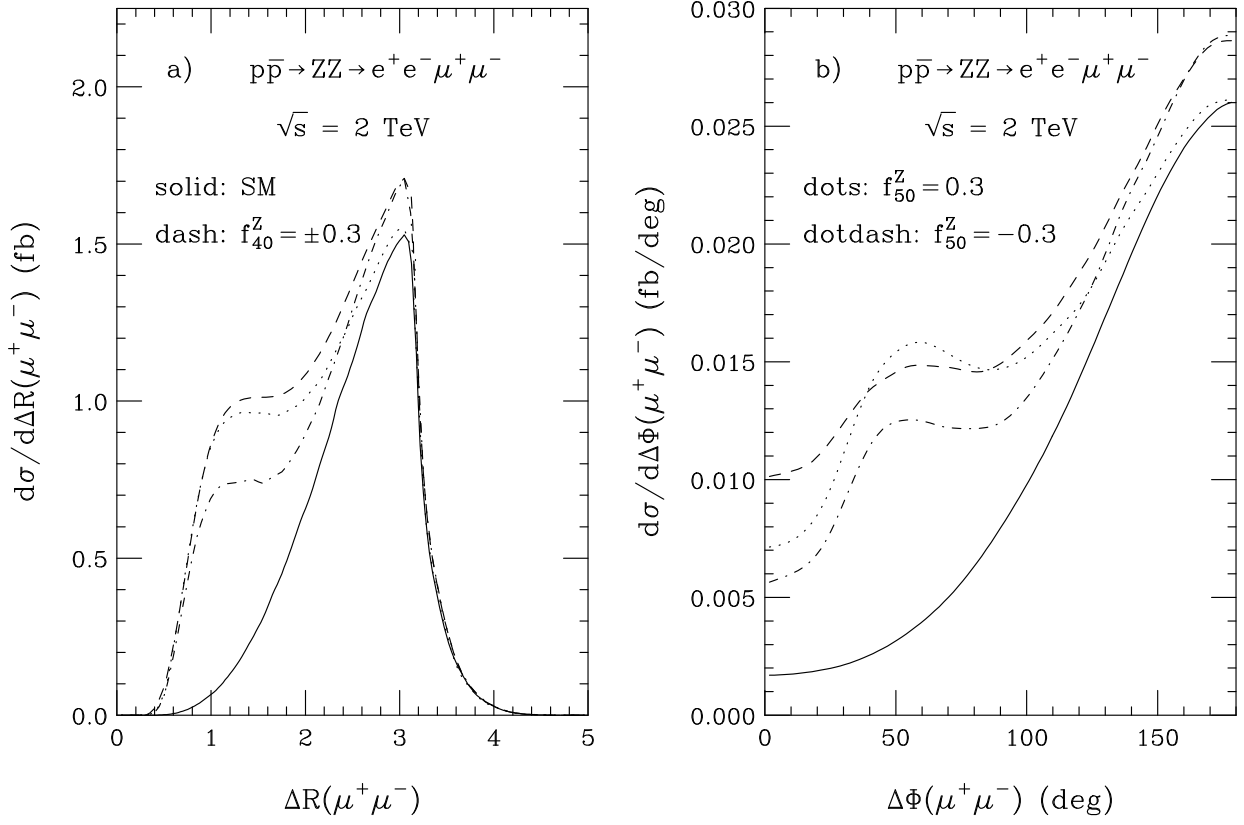


FIG. 6. The $\Delta R(\mu^+\mu^-)$ and $\Delta\Phi(\mu^+\mu^-)$ distributions in $p\bar{p} \rightarrow ZZ \rightarrow e^+e^-\mu^+\mu^-$ at the Tevatron ($\sqrt{s} = 2$ TeV) in the SM and in the presence of non-standard ZZZ couplings. The cuts imposed are described in detail in Sec. III A. The form factor scale has been set to $\Lambda_{FF} = 750$ GeV.

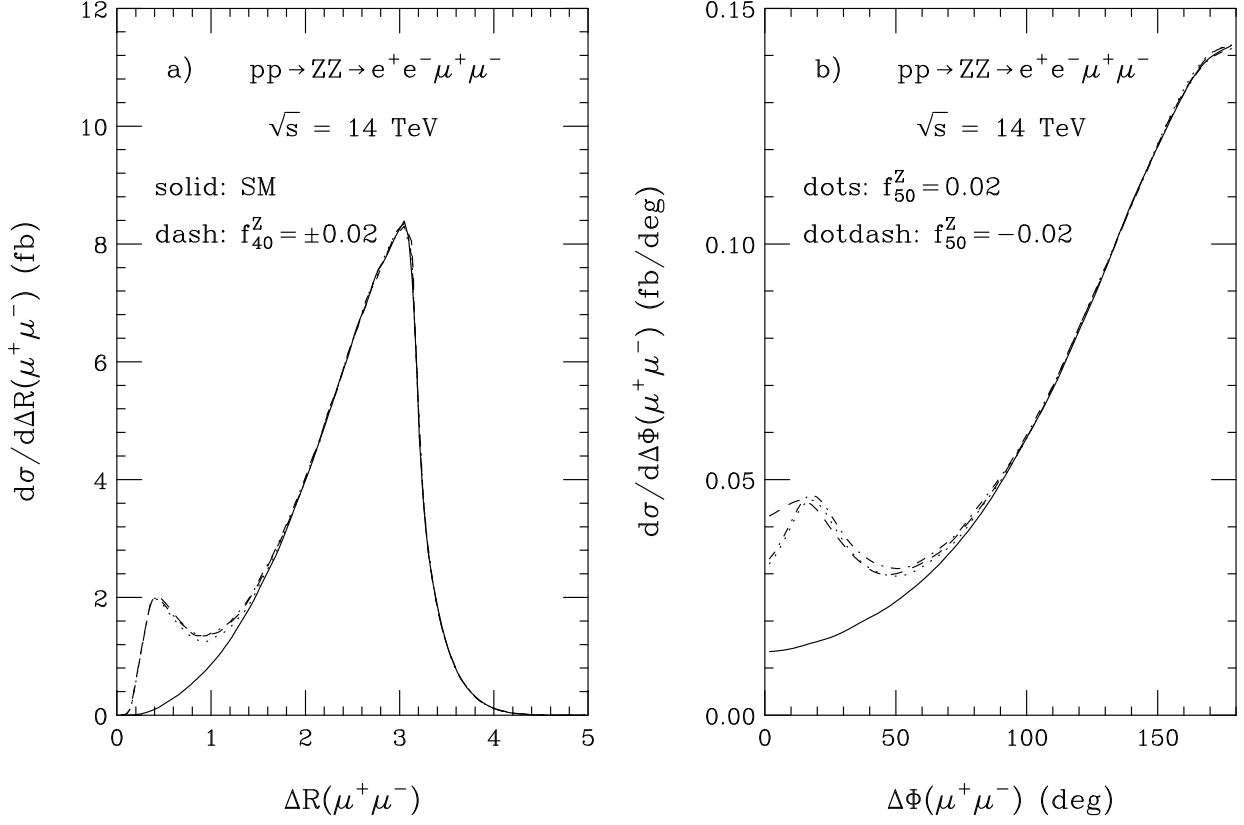


FIG. 7. The $\Delta R(\mu^+\mu^-)$ and $\Delta\Phi(\mu^+\mu^-)$ distributions in $pp \rightarrow ZZ \rightarrow e^+e^-\mu^+\mu^-$ at the LHC ($\sqrt{s} = 14$ TeV) in the SM and in the presence of non-standard ZZZ couplings. The cuts imposed are described in detail in Sec. III A. The form factor scale has been set to $\Lambda_{FF} = 2$ TeV.

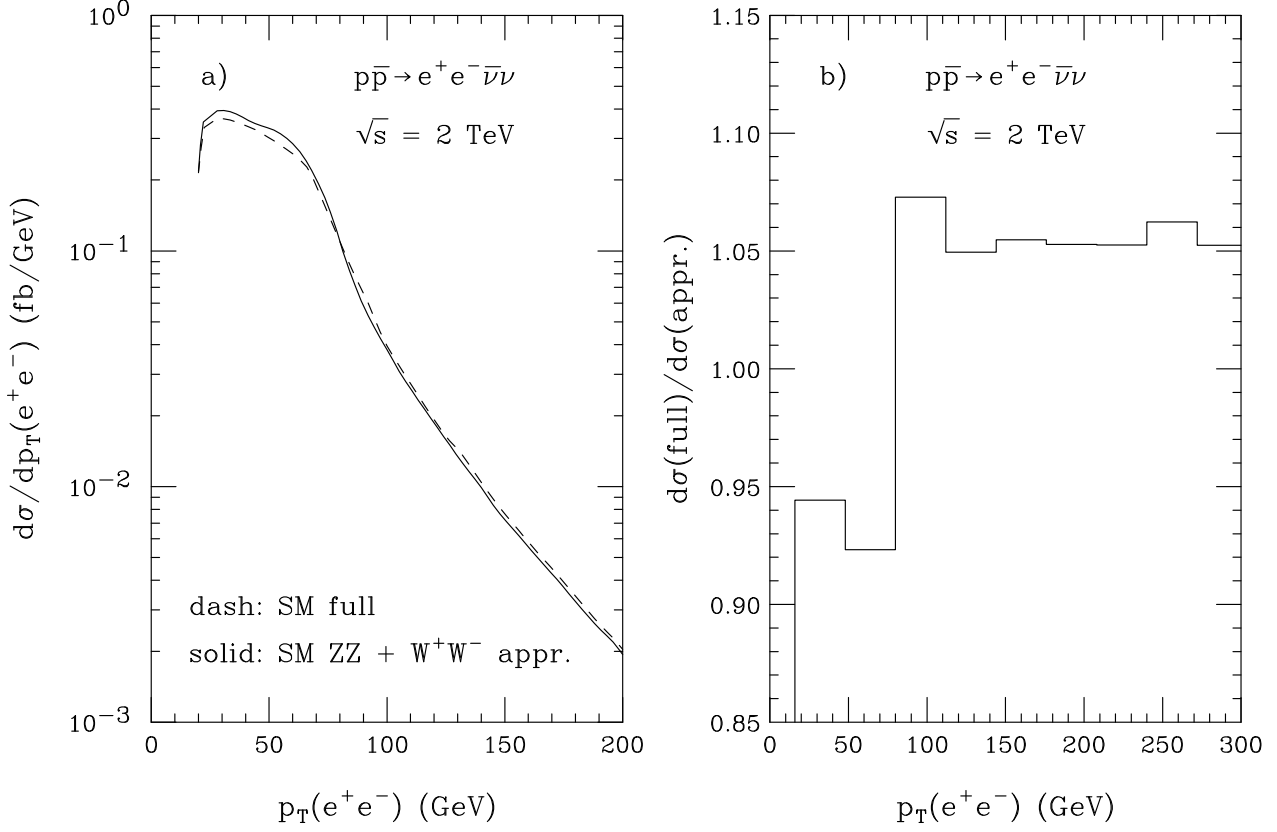


FIG. 8. Full and approximate results for the transverse momentum distribution of the e^+e^- pair in $p\bar{p} \rightarrow e^+e^-\bar{\nu}\nu$ at the Tevatron ($\sqrt{s} = 2$ TeV) in the SM. The individual distributions obtained using the full set of contributing Feynman diagrams (solid line) and the subset of diagrams for $q\bar{q} \rightarrow ZZ \rightarrow e^+e^-\bar{\nu}\nu$ and $q\bar{q} \rightarrow W^+W^- \rightarrow e^+e^-\bar{\nu}_e\nu_e$ in the double pole approximation (dashed line) are shown in part a). Part b) displays the ratio of the full and approximate differential cross sections. The cuts imposed are described in detail in the text.

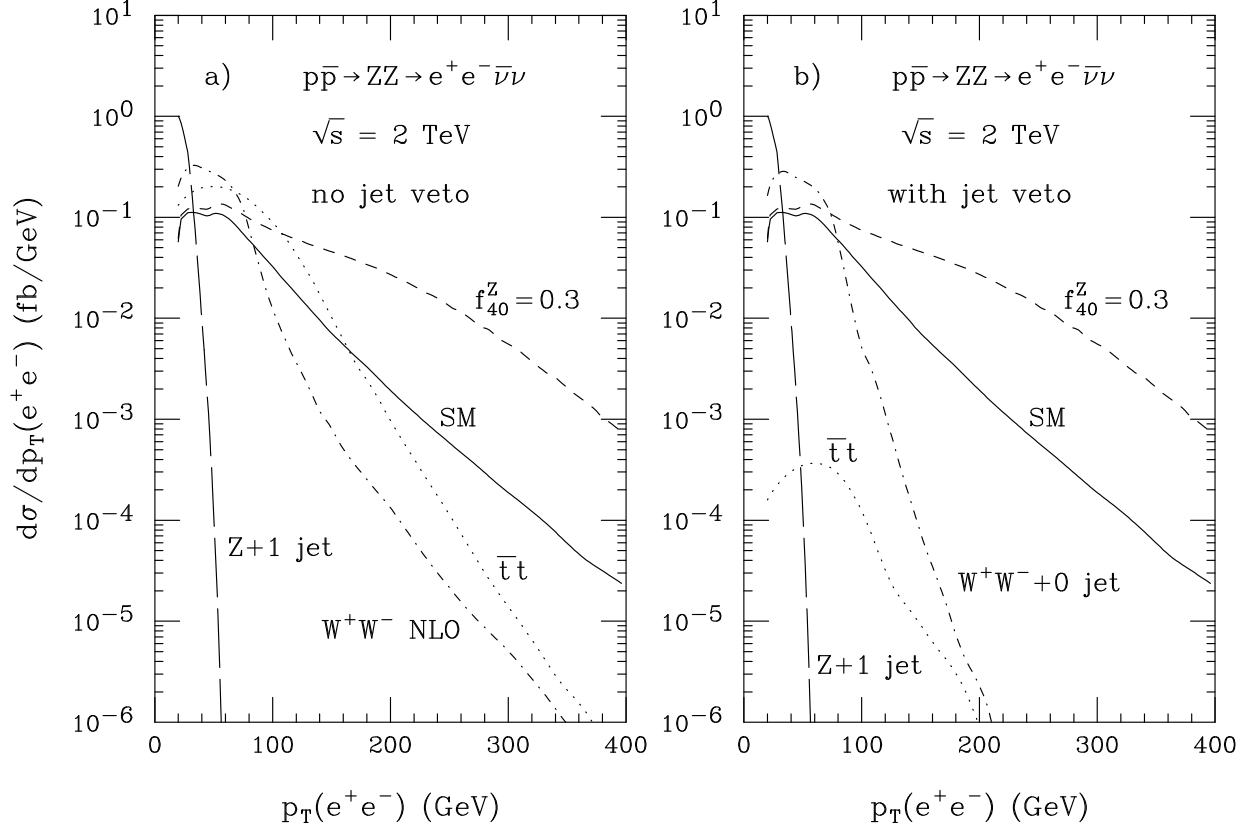


FIG. 9. Transverse momentum distribution of the e^+e^- pair in $p\bar{p} \rightarrow ZZ \rightarrow e^+e^-\bar{\nu}\nu$ at the Tevatron ($\sqrt{s} = 2$ TeV) for the SM and for $f_{40}^Z = 0.3$, together with the differential cross sections from several background processes (a) without and (b) with a jet veto applied. The cuts imposed are described in detail in the text. The form factor scale for nonzero ZZV couplings has been set to $\Lambda_{FF} = 750$ GeV.

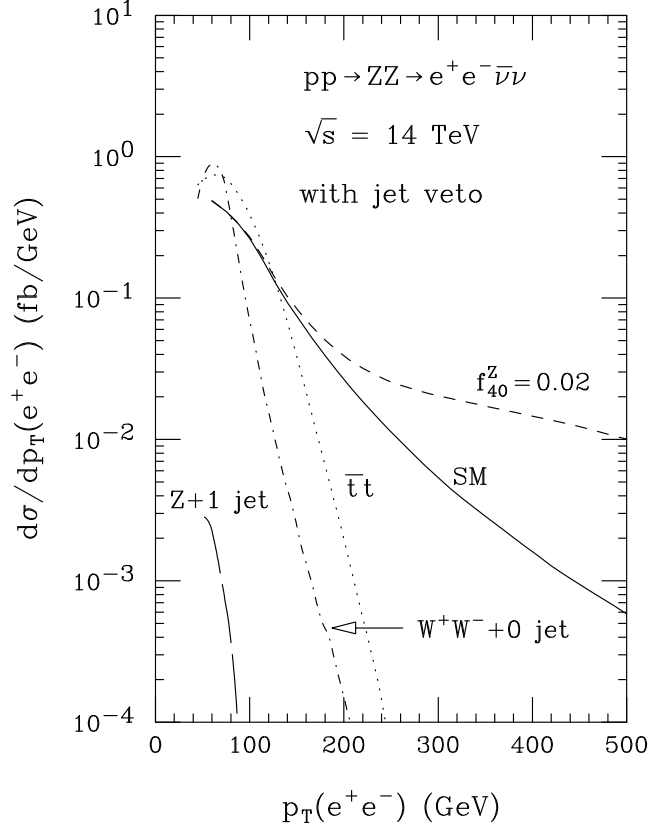


FIG. 10. Transverse momentum distribution of the e^+e^- pair in $pp \rightarrow ZZ \rightarrow e^+e^- \bar{\nu}\nu$ at the LHC ($\sqrt{s} = 14$ TeV) for the SM and for $f_{40}^Z = 0.02$, together with the differential cross sections from several background processes. The cuts imposed are described in detail in the text. The form factor scale for nonzero ZZV couplings has been set to $\Lambda_{FF} = 2$ TeV.

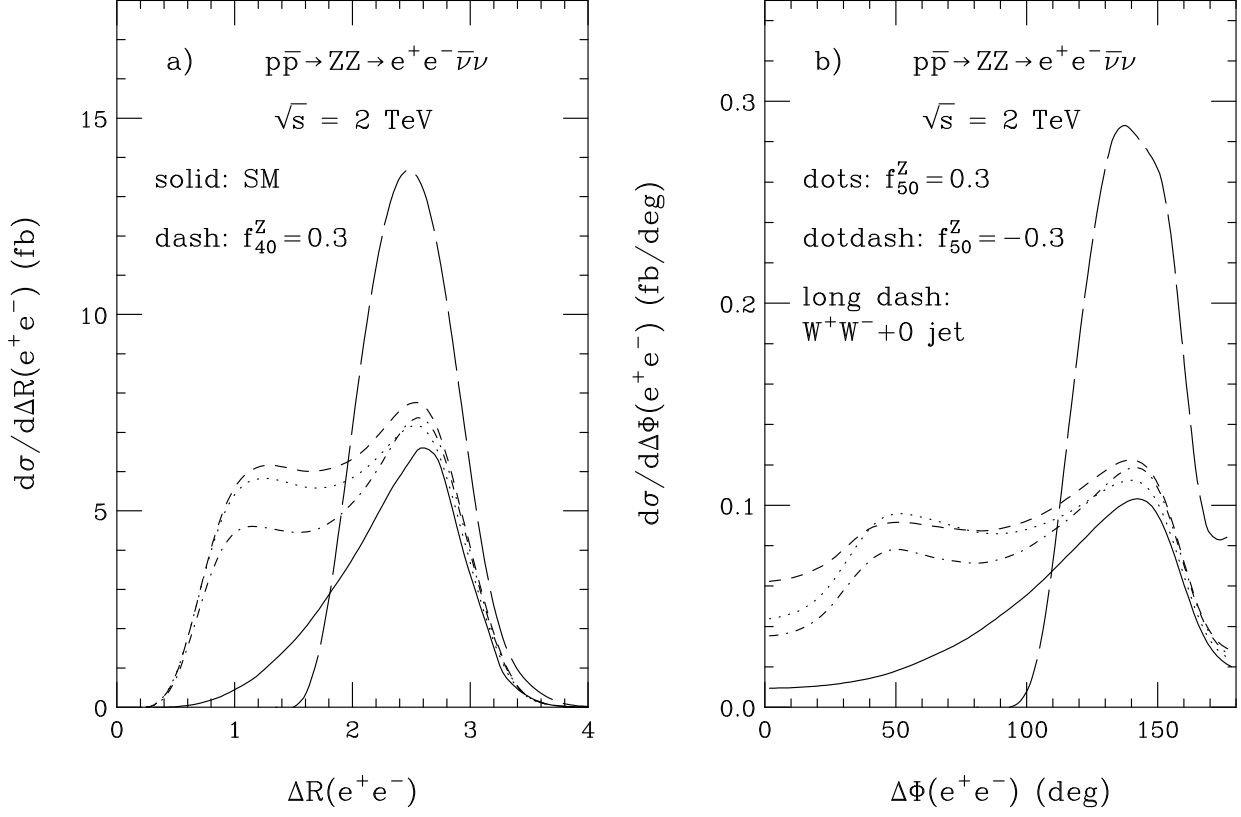


FIG. 11. The $\Delta R(e^+e^-)$ and $\Delta\Phi(e^+e^-)$ distributions in $p\bar{p} \rightarrow ZZ \rightarrow e^+e^-\bar{\nu}\nu$ at the Tevatron ($\sqrt{s} = 2 \text{ TeV}$) in the SM and in the presence of non-standard ZZZ couplings. The cuts described in Sec. III A and a $p_T > 20 \text{ GeV}$ cut are imposed. In addition, we require that no jets with $p_T(j) > 20 \text{ GeV}$ and $|\eta(j)| < 3.5$ are present. The form factor scale has been set to $\Lambda_{FF} = 750 \text{ GeV}$.

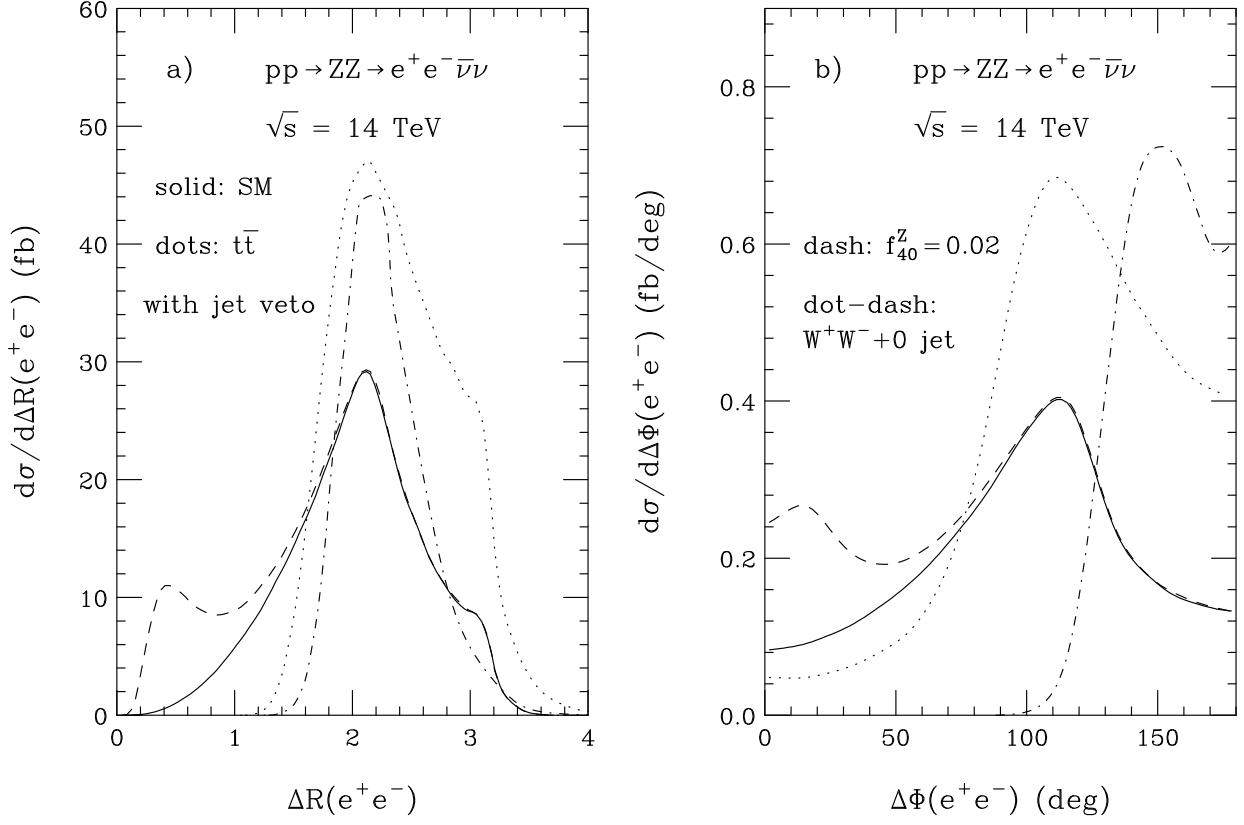


FIG. 12. The $\Delta R(e^+e^-)$ and $\Delta\Phi(e^+e^-)$ distributions in $pp \rightarrow ZZ \rightarrow e^+e^-\bar{\nu}\nu$ at the LHC ($\sqrt{s} = 14$ TeV) in the SM and for $f_{40}^Z = 0.02$ with a form factor scale of $\Lambda_{FF} = 2$ TeV. The dotted and dash-dotted curves represent the $t\bar{t}$ and $W^+W^- + 0$ jet backgrounds. The cuts described in Sec. III A and a $p_T > 50$ GeV cut are imposed. In addition, we require that no jets with $p_T(j) > 50$ GeV and $|\eta(j)| < 5$ are present.

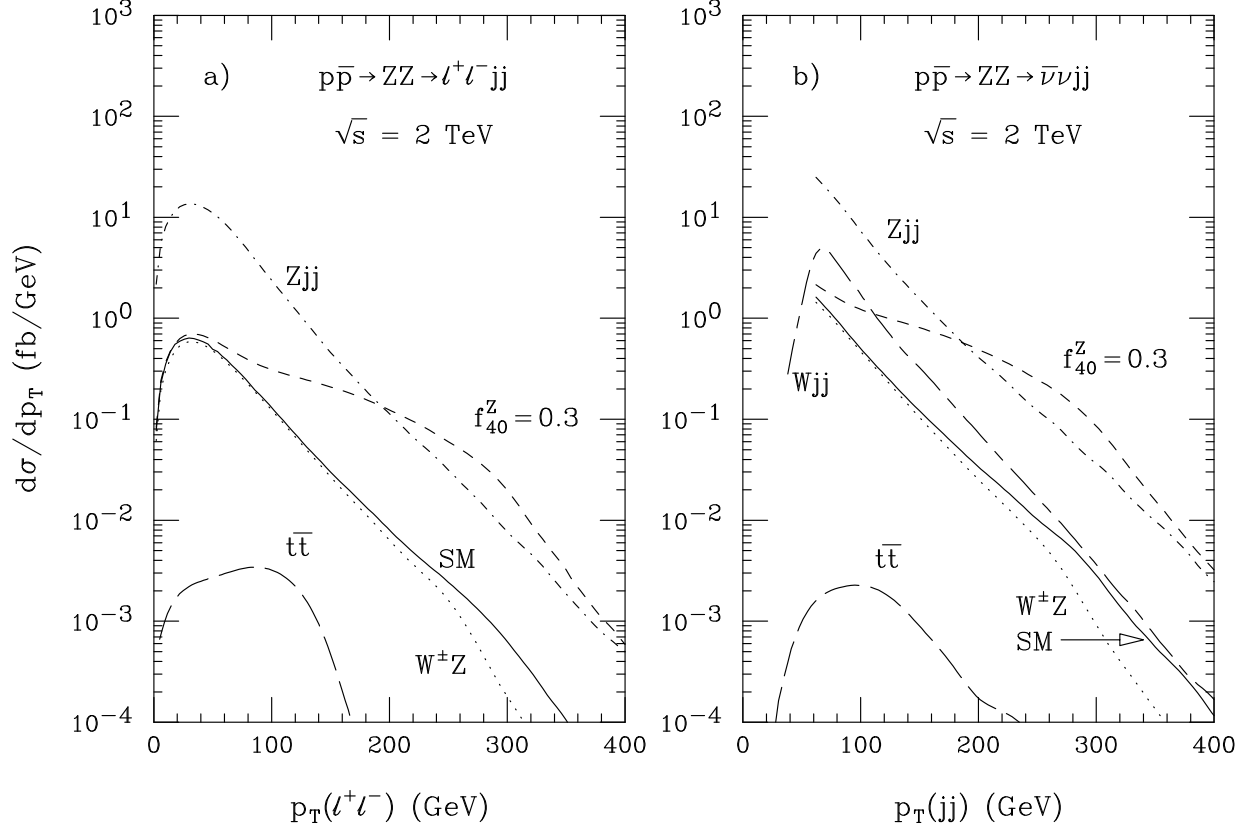


FIG. 13. Transverse momentum distribution (a) of the $\ell^+\ell^-$ pair in $p\bar{p} \rightarrow ZZ \rightarrow \ell^+\ell^- jj$, and (b) of the jet pair in $p\bar{p} \rightarrow ZZ \rightarrow \bar{\nu}\nu jj$, at the Tevatron ($\sqrt{s} = 2$ TeV). The SM prediction is shown together with the cross section for $f_{40}^Z = 0.3$ and $\Lambda_{FF} = 750$ GeV. Also shown are the differential cross sections of various background processes. The cuts imposed are described in detail in the text.

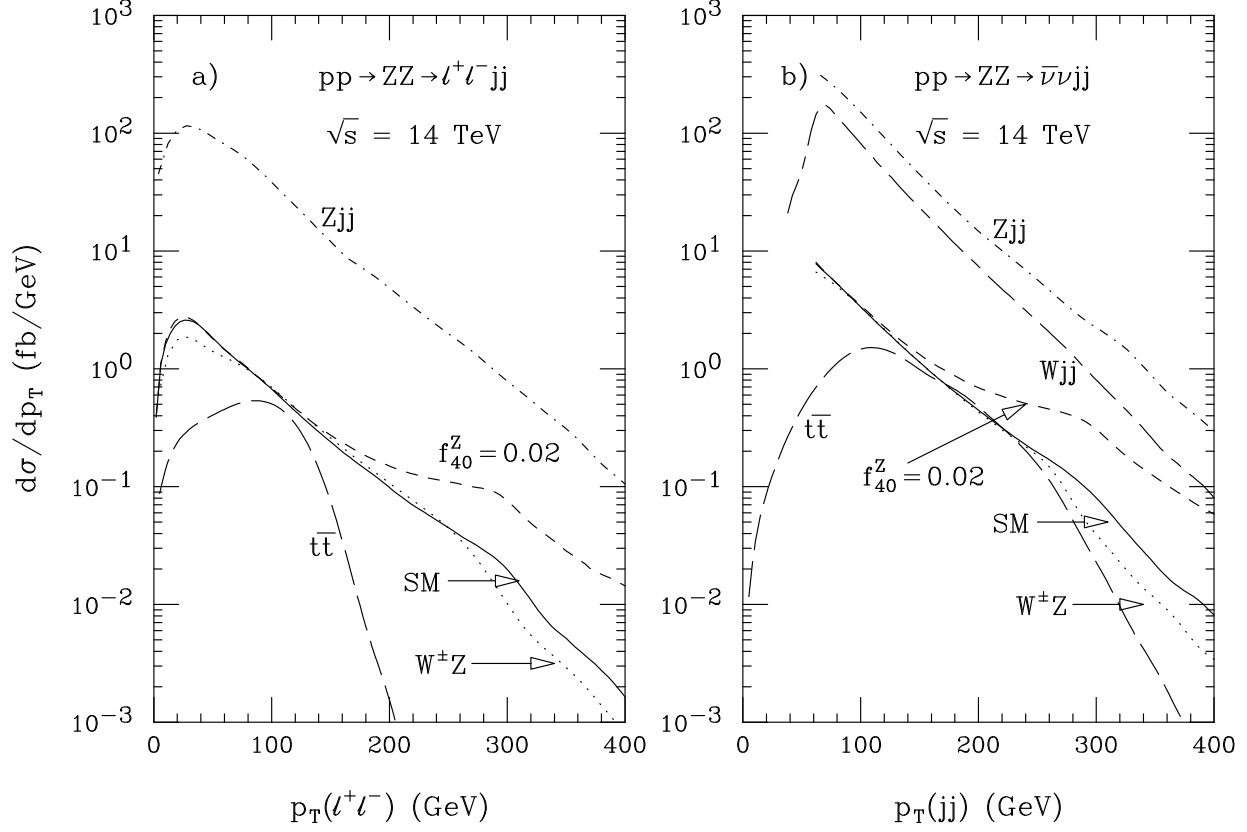


FIG. 14. Transverse momentum distribution (a) of the $\ell^+\ell^-$ pair in $pp \rightarrow ZZ \rightarrow \ell^+\ell^- jj$, and (b) of the jet pair in $pp \rightarrow ZZ \rightarrow \bar{\nu}\nu jj$, at the LHC ($\sqrt{s} = 14$ TeV). The SM prediction is shown together with the cross section for $f_{40}^Z = 0.02$ and $\Lambda_{FF} = 2$ TeV. Also shown are the differential cross sections of various background processes. The cuts imposed are described in detail in the text.

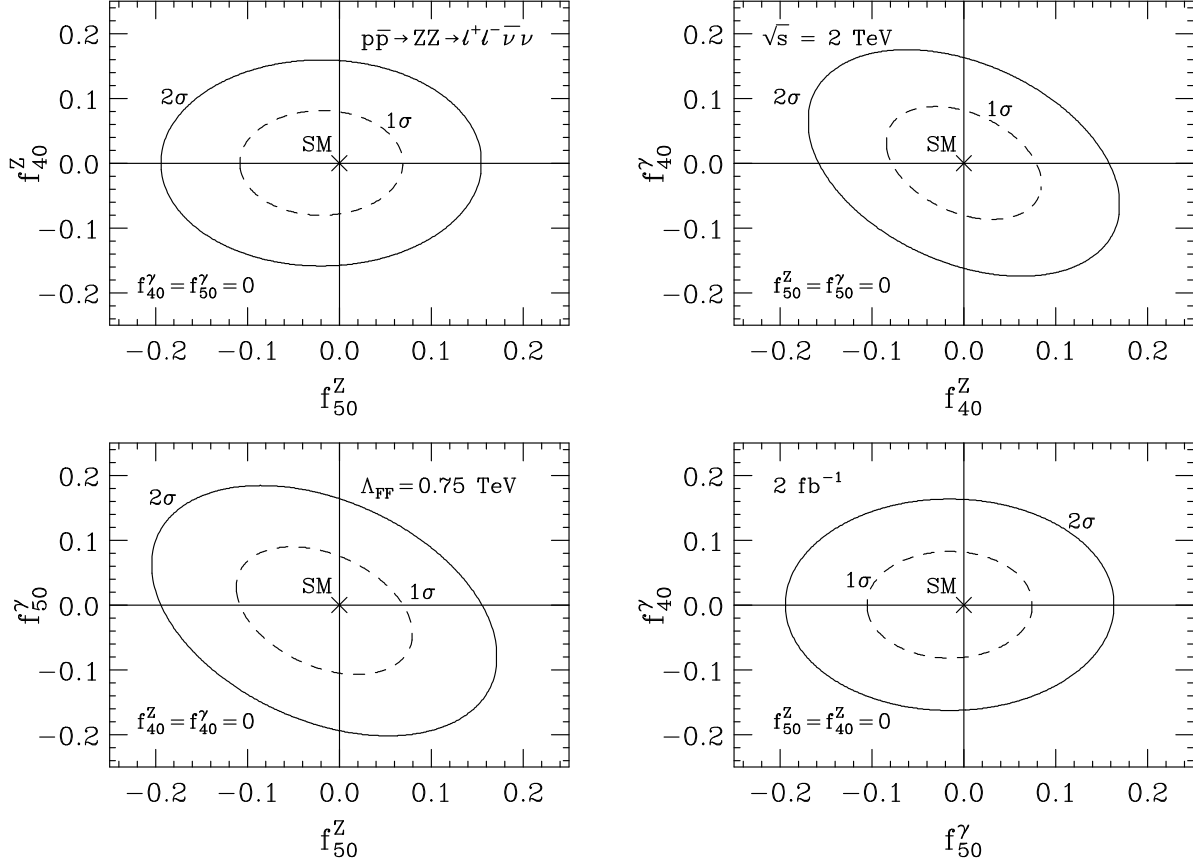


FIG. 15. Correlated sensitivity limits for ZZV anomalous couplings in $p\bar{p} \rightarrow ZZ \rightarrow \ell^+ \ell^- \bar{\nu} \nu$ events at the Tevatron Run II ($\sqrt{s} = 2$ TeV) with 2 fb^{-1} of data. All couplings are assumed to be real. Shown are 1σ (dashed lines) and 2σ (solid lines) limit contours of all combinations of f_{i0}^Z versus f_{i0}^γ ($i = 4, 5$). A form factor scale of $\Lambda_{FF} = 750$ GeV has been assumed. In each graph, only those couplings which are plotted against each other are assumed to be different from their zero SM values.